MERCURY CADMIUM TELLURIDE PHOTODIODE

D.A. Soderman
A.B. Timberlake
Honeywell Radiation Center
2 Forbes Road
Lexington, Massachusetts 02173

November 1970
Interim Report for Period May - November 1970

Prepared for

GODDARD SPACE FLIGHT CENTER
Greenbelt, Maryland 20771

1. Report No.	2. Government Accession No.	3. Recipient's Catalog No.

4. Title and Subtitle	5. Report Date
Mercury Cadmium Telluride Photodiode	November 1970
	6. Performing Organization Code
7. Author(s) D. A. Soderman and A. B. Timberlake	8. Performing Organization Report No.
9. Performing Organization Name and Address Honeywell Radiation Center 2 Forbes Road Lexington, Massachusetts 02173	10. Work Unit No.
	11. Contract or Grant No. NAS 5-21197
12. Sponsoring Agency Name and Address Goddard Space Flight Center Greenbelt, Maryland 20771	13. Type of Report and Period Covered Interim Report May - November 1970
	14. Sponsoring Agency Code

15. Supplementary Notes

16. Abstract

17. Key Words	18. Distribution Statement
Infrared photodiode Mercury cadmium telluride	

19. Security Classif. (of this report)	20. Security Classif. (of this page)	21. No. of Pages	22. Price

PREFACE

This report, submitted February 1971, describes work performed under contract NAS5-21197 during the period from May 1970 through November 1970. The program has been conducted at the Honeywell Radiation Center, Lexington, Massachusetts. The NASA program monitors have been Mr. J. McElroy and S. Cohen at the Goddard Space Flight Center.

A number of scientists and technicians have contributed to the program. Dr. D. A. Soderman and Mr. A. B. Timberlake were the principal investigators. Mr. R. Lancaster and Dr. H. A. Andrews supported this program through the (Hg,Cd)Te material growth and characterization. Mr. D. Maloney fabricated the devices. We acknowledge the valuable technical discussions with Drs. J. B. Flynn and M. W. Scott.

ABSTRACT

High speed sensitive (Hg,Cd)Te photodiode detectors operating in the 77 to 90 °K temperature range have been developed for the 10.6 μm spectral region, P-N junctions formed by impurity (gold) diffusion in n-type (Hg,Cd)Te and by stoichiometric deviation (mercury) diffusion in p-type (Hg,Cd)Te have been investigated. These photodiodes of approximately 3×10^{-3} cm^2 area have exhibited responsivities between 20 and 360 V/W, external quantum efficiencies between 2 and 50%, specific detectivities D^*_λ (11.5, 1 kHz, 1 Hz) between 0.7 and 1.7×10^{10} cm $Hz^{1/2}/W$, and response times between 40 and less than 7 nanoseconds (25 MHz) which is frequency limitation of the CO_2 laser heterodyne system.

TABLE OF CONTENTS

SECTION 1

INTRODUCTION AND SUMMARY

Advanced high data rate, intersatellite communications systems envisioned and under construction by NASA/Goddard Space Flight Center will require highly sophisticated infrared detectors. In order to utilize the capabilities of the CO_2 laser fully, a photodetector sensitive to 10.6-μm radiation with an electrical bandwidth in the GHz range must be developed. Furthermore, for the detector to be useful in spacecraft systems, it should not require cooling below liquid nitrogen temperature.

Although there are 10.6-μm photodetectors with properties which approach some of the electrical bandwidth, quantum efficiency, and temperature requirements, there are none which meet all of these. Thus, Honeywell has been engaged in a program with NASA/Goddard to develop a mercury cadmium telluride photodiode with a 3-dB roll-off frequency greater than 400 MHz, a quantum efficiency of 20% and an operating temperature of 100 °K. To achieve this design goal, Honeywell has directed its efforts first towards producing photodiodes with consistent, reproducible characteristics and then towards optimizing those characteristics to meet the goals of this effort.

The material properties of the alloy semiconductor mercury cadmium telluride (Hg,Cd)Te are ideally suited to this application because of the following characteristics: (1) a continuously variable energy gap, permitting the peak responsivity to be tuned to 10.6 μm; (2) an intrinsic photodetector, allowing high performance operation in the 77 to 100 °K temperature range; (3) a direct low energy gap semiconductor, leading to a high absorption coefficient and resulting in a very high quantum efficiency; (4) a high electron mobility, yielding very short transit times and a large electrical bandwidth; and (5) a well-established material growth and detector fabrication technology, yielding high performance (Hg,Cd)Te photoconductive detectors for the 8-14 μm spectral region.

During the first phase of this contract, Honeywell has made substantial progress in the investigation of (Hg,Cd)Te material properties and diffusion techniques required for the fabrication of high speed (Hg,Cd)Te photodiodes. Temperature dependent Hall coefficient and resistivity measurements have been made to select classical n and p-type (Hg,Cd)Te. P-N junctions have been formed by impurity (gold) diffusion in n-type material and by stoichiometric deviation (mercury) diffusion in p-type material. Radioactive tracer and electrical measurements on the diffused surface layer have suggested a two-step diffusion mechanism in (Hg,Cd)Te material.

One gold diffused photodiode at 77 °K with an 11.5 μm peak spectral response and 4 x 10^{-3} cm^2 area exhibited responsivity between 100 and 360 V/W, external quantum efficiency between 16 and 50%, specific detectivity between 0.7 and 1.7 x 10^{10} cm $Hz^{1/2}/W$, and 40-nanosecond response time with 0.9 μm radiation. These performance characteristics vary with dc reverse bias; however, they do not change as the detector operating temperature is increased to 90 °K. The response time is limited by electrical circuit constraints through the product of the junction capacitance and series resistance of the particular contact configuration on the diffused layer which has not been optimized for high speed operation.

The reverse bias currents in the fabricated photodiodes are larger than expected at low temperatures; thus, several experiments to investigate surface inversion and bulk diffusion material properties have been initiated. Voltage dependent junction capacitance and resistance measurements have been made to further the understanding of the junction characteristics.

The performance of photodiodes fabricated by mercury in-diffusion (stoichiometric deviation) has not been as extensively analyzed as the gold diffused photodiodes, however the zero bias responsivity and detectivity measurements made on a number of photodiodes with peak spectral responses in the 8.6 to 11.5-μm range are encouraging. The zero bias performance characteristics of several mercury diffused photodiodes at 77 °K have shown responsivities between 20 and 200 V/W, external quantum efficiencies between 2 and 24%, and specific detectivities as high as 1.5 x 10^{10} cm $Hz^{1/2}/W$. Response time measurements were made using pulsed 0.9-μm radiation ranging from 20 to 50 nanoseconds and CO_2 laser (10.6-μm radiation) heterodyne detection ranging from 16 nanoseconds to less than 7 nanoseconds. The heterodyne laser equipment limited this frequency response measurement to 25 MHz.

SECTION 2

MATERIAL PROPERTIES OF (Hg,Cd)Te

Before a high speed (Hg,Cd)Te photodiode can be designed for a peak responsivity at 10.6 μm and its performance predicted, several material parameters must be established. The following calculations for the effective mass, intrinsic carrier concentration, mobility, and lifetime have been previously reported under prior NASA and Air Force contracts and have been included in this report to establish a firm theoretical understanding of the material parameters of (Hg,Cd)Te.

2.1 ENERGY GAP

Mercury cadmium telluride $(Hg_{1-x}Cd_x)Te$ is a ternary alloy formed by chemically combining the semi-metal mercury telluride (HgTe) with the semiconductor cadmium telluride (CdTe). In this notation, x represents the mole fraction of CdTe. A continuously variable optical bandgap in (Hg,Cd)Te can be produced because this material has a bandgap contraction and inversion as a function of composition. In particular, the bandgap can be varied from 1.6 eV to approximately zero eV.

This large variation is possible because the two compounds are completely miscible for x values between 0 and 1. Since the bandgaps of both HgTe and CdTe are temperature dependent, the bandgap of the alloy varies with temperature as well as with composition. Figure 2.1 shows the most probable dependence of the $\Gamma 6 - \Gamma 8$ bandgap (henceforth called E_g) upon x inferred from recent optical absorption and detector cutoff wavelength measurements over a large range of x values.

To create electron hole pairs by intrinsic absorption of 10.6-μm radiation from a CO_2 laser, an energy gap near 0.1 eV is required. Thus, the $(Hg_{1-x},Cd_x)Te$ material should be prepared with an x value near 20%. Since the energy gap varies significantly with temperature in this composition range, a more precise composition for 10.6-μm peak sensitivity depends on the detector temperature.

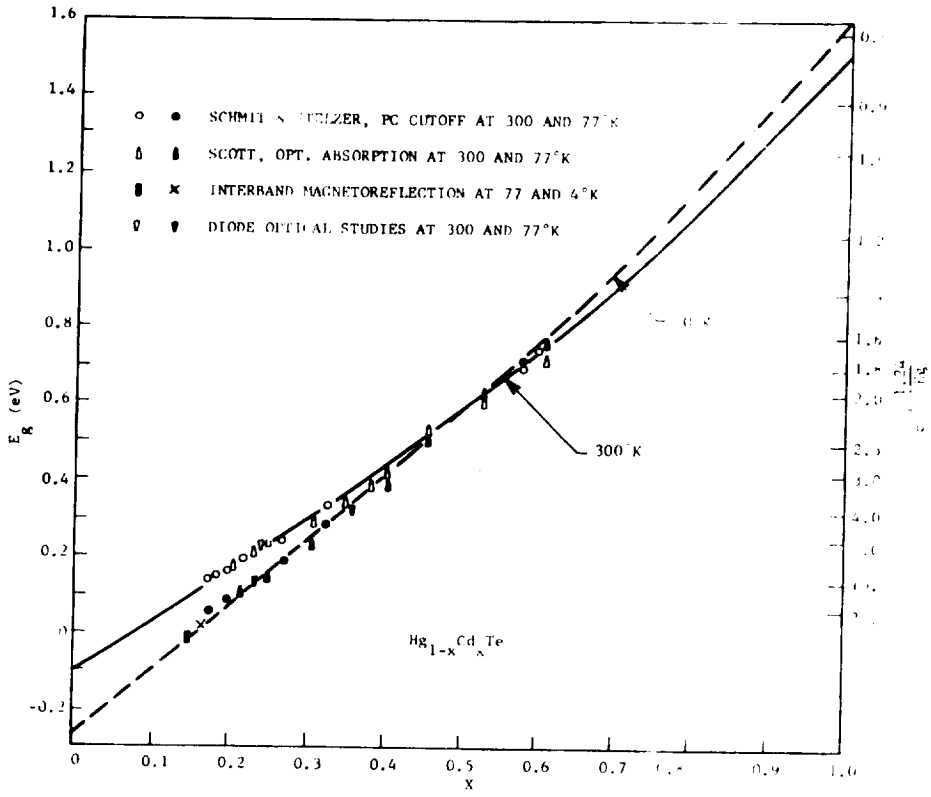

Figure 2.1 ENERGY GAP VS COMPOSITION IN $(Hg_{1-x}Cd_x)Te$

The compositional and linear temperatures of the energy gap as determined by detector cutoff wavelengths are given by Schmit and Stelzer[1] as:

$$Eg(eV) = 1.59\ x - 0.25 + 5.23\ (10^{-4})T(1-2.08\ x) + 0.327\ x^3 \qquad (2.1)$$

M.W. Scott[2] gives an expression for the temperature dependence of the energy gap as determined by optical absorption which differs from equation 2.1 by at most a few hundredths of an eV at low x values.

2.2 OPTICAL ABSORPTION COEFFICIENT

The optical absorption coefficient versus wavelength has been calculated from the infrared transmission through a 20-μm thick sample of $(Hg_{0.79},Cd_{0.21})Te$ at 87 °K. These results are shown in Figure 2.2. Except for the shift in wavelength due to the temperature dependence of the energy gap, the shape of this curve does not vary significantly with temperature[3]. Also shown in Figure 2.2 is the extrapolated optical absorption versus wavelength for the approximate composition of (Hg,Cd)Te required for 10.6-μm radiation detection. The optical absorption coefficient for this composition $(Hg_{.805},Cd_{0.195})Te$ at 87 °K should be at least 2×10^3 cm^{-1} for 10.6-μm radiation. This absorption curve and others made at different temperatures and compositions can be approximated by the expression given by Stern[4] for a simple band structure:

$$\alpha(\lambda) = \frac{3.38 \times 10^5}{n} \left(\frac{m_c}{m}\right)^{1/2} \frac{E_g \lambda}{hc} \left\{\frac{hc}{\lambda} - E_g\right\}^{1/2} \qquad (2.2)$$

This absorption coefficient should be insensitive to conductivity type. In p-type material, where there should be a negligible Burstein-Moss shift, the absorption coefficient should be insensitive to doping concentration.

2.3 EFFECTIVE MASS AND INTRINSIC CARRIER CONCENTRATION

Values for the electron effective mass (m_e^*) as a function of composition x and temperature have been calculated by J. Schmit[5] from the temperature dependence of the energy gap using the Kane[6] model for degenerate nonparabolic bands. The nonparabolicity

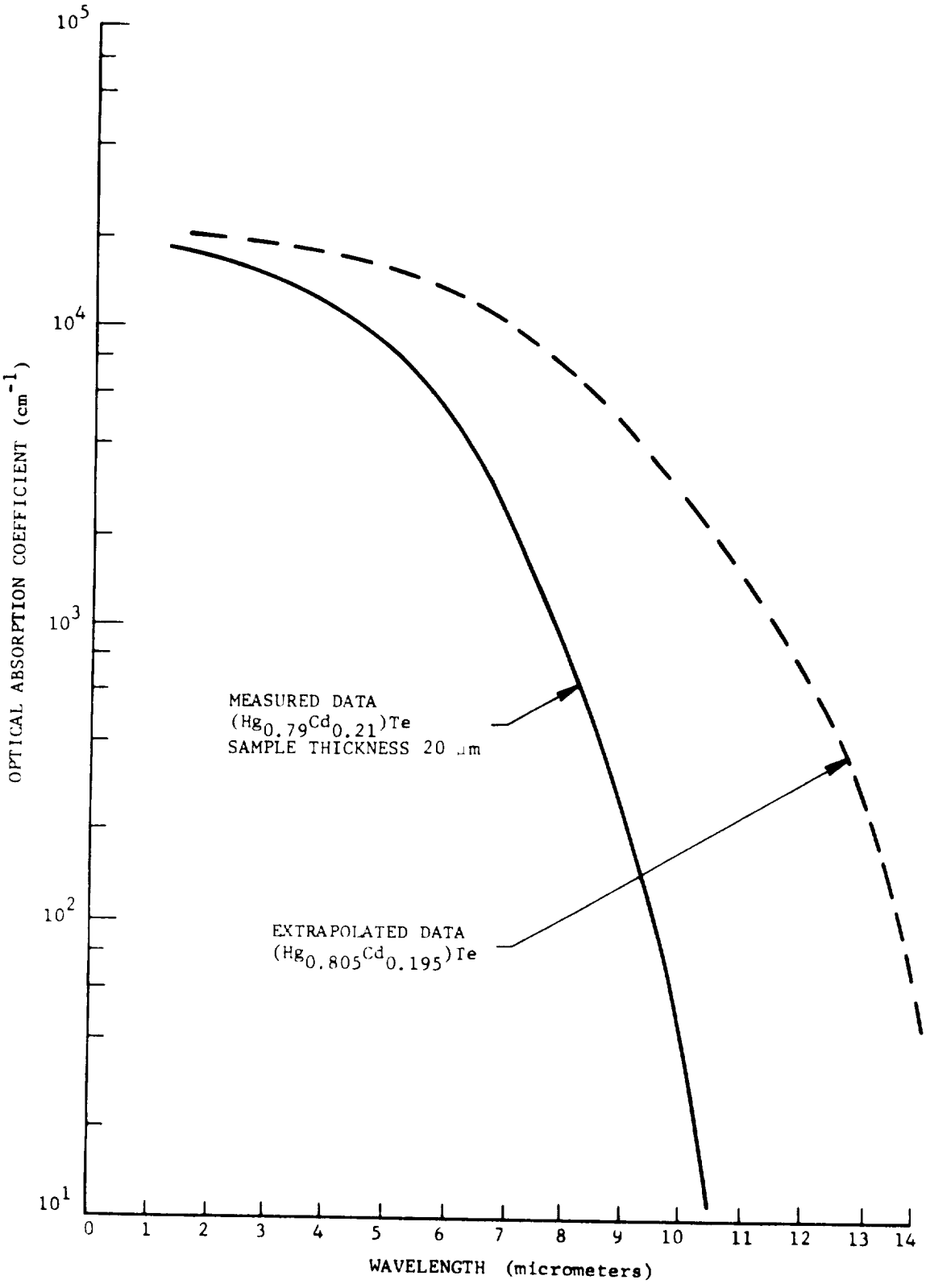

Figure 2.2 OPTICAL ABSORPTION COEFFICIENT VS WAVELENGTH AT 87°K

of the conduction band causes large changes in m_e^* with (Hg,Cd)Te composition and temperature. The m_e^* is obtained by setting equal the classical and Kane carrier concentration expressions. The results shown in Figure 2.3 have been obtained by calculating the energy gap, and then the reduced Fermi level is varied until a numerical integration yields $n = p = n_i$.

$$n_i = 1.99 \times 10^{15} T^{3/2} (m_e^*/m_o)^{3/4} \exp(-Eg/2kT) \quad (2.3a)$$

$$n_i = 8.1686 \times 10^{7} T^{3} \int_o^\infty \frac{\sqrt{\gamma(\gamma + Eg/kT)}\ (2\gamma + Eg/kT)d\gamma}{1 + \exp(\gamma - \varphi/dT)} \quad (2.3b)$$

In these equations γ is a variable of integration which includes the Kane matrix element = 9×10^{-8} eV cm, and φ is the reduced Fermi energy measured from the conduction band. T represents the detector temperature and n_i the intrinsic free-carrier concentration. The temperature and composition dependence of electron effective mass and intrinsic carrier concentration are shown in Figures 2.3 and 2.4. Thus, in the temperature range 77° to 140°K, the electron effective mass for x = 0.2 material is roughly 0.008 μm_o and the intrinsic carrier concentration is roughly 2×10^{14} cm^{-3}.

The following assumptions have been made in this calculation: (1) linear temperature dependence of E_g, (2) validity of Kane $\vec{k} \cdot \vec{p}$ model as formulated by Harman and Strauss, and (3) hole effective mass $m_h^* = 0.55\ m_o$ which is independent of composition and temperature. The density-of-states electron effective mass calculated in this model agrees reasonably well with the (conductivity) effective mass measured from the cyclotron resonance absorption[8,9,10].

2.4 MOBILITY AND DEGENERACY

In (Hg,Cd)Te, the major scattering process determining the mobility includes both impurity and lattice scattering. In the temperature range between 100 and 300 °K, the lattice scattering of free carriers decreases as the temperature is lowered. Acoustic and

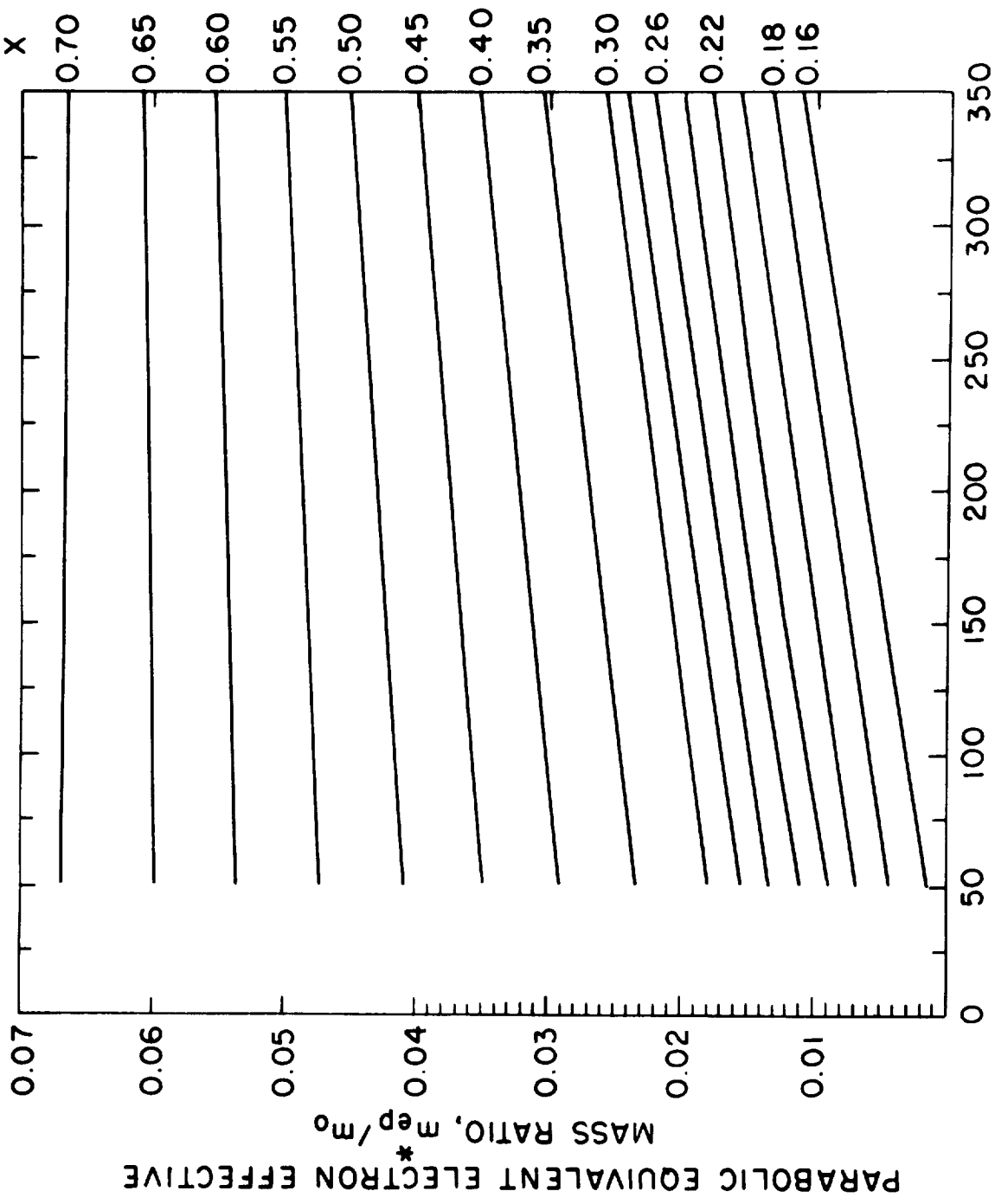

Figure 2.3 TEMPERATURE DEPENDENCE OF THE ELECTRON EFFECTIVE MASS OF $Hg_{1-x}Cd_xTe$ CALCULATED FROM n_i

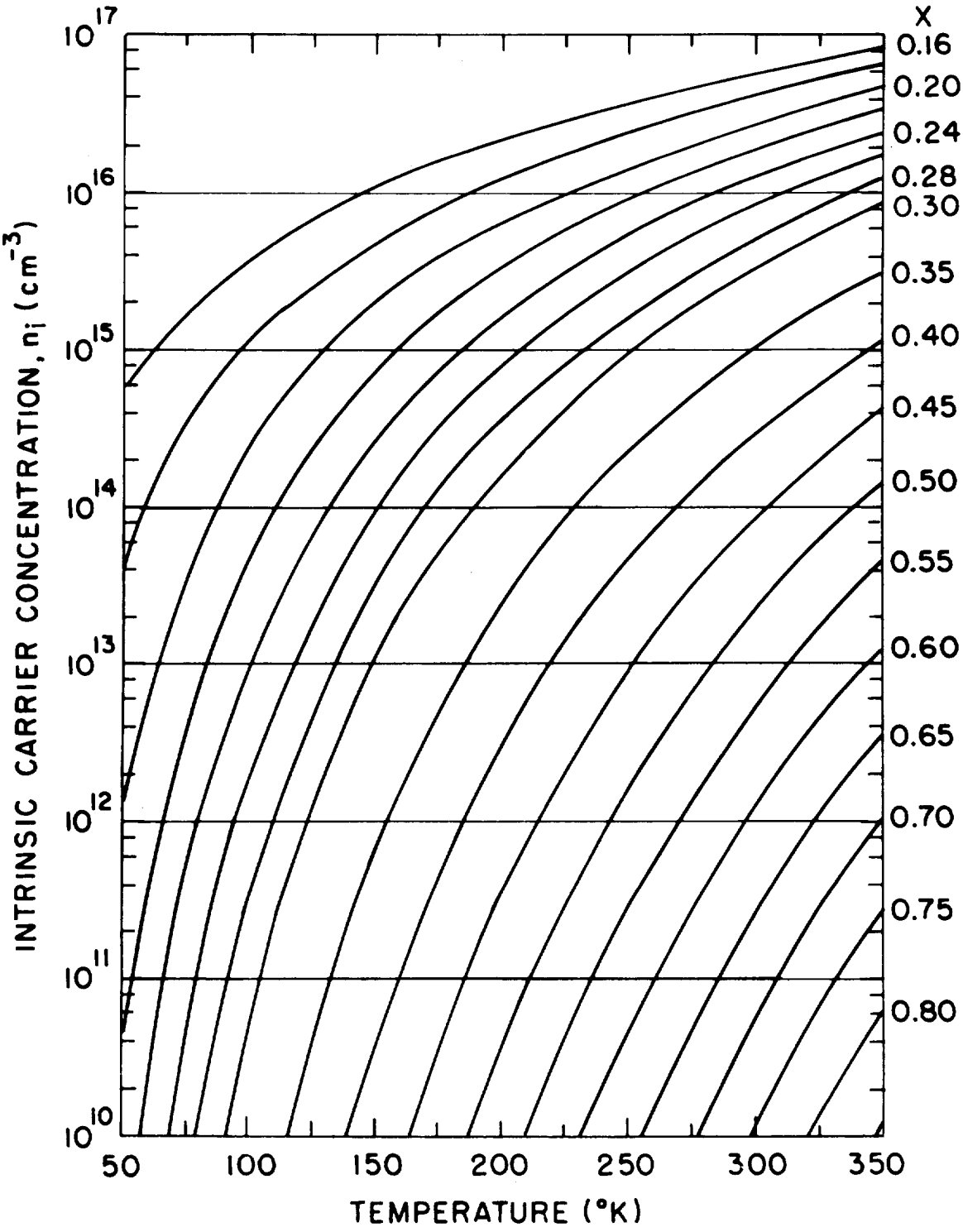

Figure 2.4 CALCULATED TEMPERATURE DEPENDENCE OF THE INTRINSIC CARRIER CONCENTRATION OF $Hg_{1-x}Cd_xTe$ FOR $0.16 \leq x \leq 0.80$

optical phonon (lattice) scattering in n-type material has an effective mass and temperature dependence given by

$$\mu_{lattice} \propto \frac{1}{(m_e^*)^{5/2} T^{3/2}} \qquad (2.4)$$

At lower temperatures the mobility peaks and eventually decreases due to scattering from ionized impurities and lattice imperfections. Calculations have been made using lattice scattering and degenerate impurity scattering over a wide range of temperatures and compositions. A partially degenerate condition exists for $x \leq 0.2$ over the temperature range from 4 to 300 °K. A free carrier concentration as high as 2×10^{15} cm^{-3} for n-type and 4×10^{17} cm^{-3} for p-type can be used in (Hg,Cd)Te without full degeneracy occurring over the 77 to 140 °K temperature range.

The electron mobility calculated from the measured Hall coefficient and resistivity in n-type $N_D \sim 5 \times 10^{14}$ cm^{-3} $(Hg_{0.81},Cd_{0.19})Te$ material having a peak spectral response at 14 μm is approximately 2×10^5 cm^2/volt-s at 77 °K. There is no distinction between the Hall and conductivity mobilities due to the spherical energy surfaces and degenerate statistics involved.

The hole mobility is not as well known in n-type (Hg,Cd)Te material. However, from photoconductive detector performance measurements made at low temperatures, the mobility ratio $\mu_e/\mu_n = b$ is roughly 10. It is not expected that the mobility ratio will be strongly temperature dependent. Thus, the hole mobility should be near 10^4 cm^2/volt in the desired temperature range.

2.5 LIFETIME

In a direct bandgap material, such as (Hg,Cd)Te, the lifetime is composed of several competing mechanisms and can be written as

$$\frac{1}{\tau} = \frac{1}{\tau_{rad}} + \frac{1}{\tau_A} + \frac{1}{\tau_{S\text{-}R}} + \frac{S}{d} \qquad (2.5)$$

where τ_{rad} is the radiative, τ_A is the Auger, and τ_{S-R} is the Shockley-Read free carrier recombination lifetimes. The S/d term includes the effect of surface recombination.

The radiative lifetime has been calculated from the Shockley and vanRoosbroeck theory using the measured absorption coefficient. The values obtained are an order of magnitude above the measured values; and, thus, $\tau_{radiative}$ can probably be neglected under most operating conditions.

The temperature dependence of the photoconductive lifetime τ in $(Hg_{0.81},Cd_{0.19})Te$ material with a 4×10^{14} cm^{-3} donor impurity concentration has been computed from the measured frequency response to a 0.9-μm radiation signal.[11] These results are shown in Figure 2.5. The temperature dependent behavior of the lifetime indicates that the τ_{S-R} is the dominant lifetime below approximately 100 °K and τ_{Auger} is the dominant lifetime at higher temperatures. Since the Shockley-Read model roughly fits the curve below 100 °K, it implies that a recombination level exists within the material and has an energy of excitation of approximately 0.02 eV. These recombination centers are believed to result from a deficiency or surplus of mercury atoms since stoichiometric deviations can produce either acceptor or donor states in the forbidden gap yielding p- and n-type material.

In Auger recombination, the lifetime will decrease as the free carrier concentration increases, as given by:

$$\tau_{Auger} = \frac{2n_i^2 \tau_i}{(n_o + p_o + \Delta n)\,[n_o + \Delta n + \beta\,(p_o + \Delta_n)]} \qquad (2.6)$$

where

τ_i = intrinsic material lifetime

β = parameter depending on the effective mass and the energy gap

Δn = background generated carriers

n_o, p_o = thermal equilibrium generated carriers

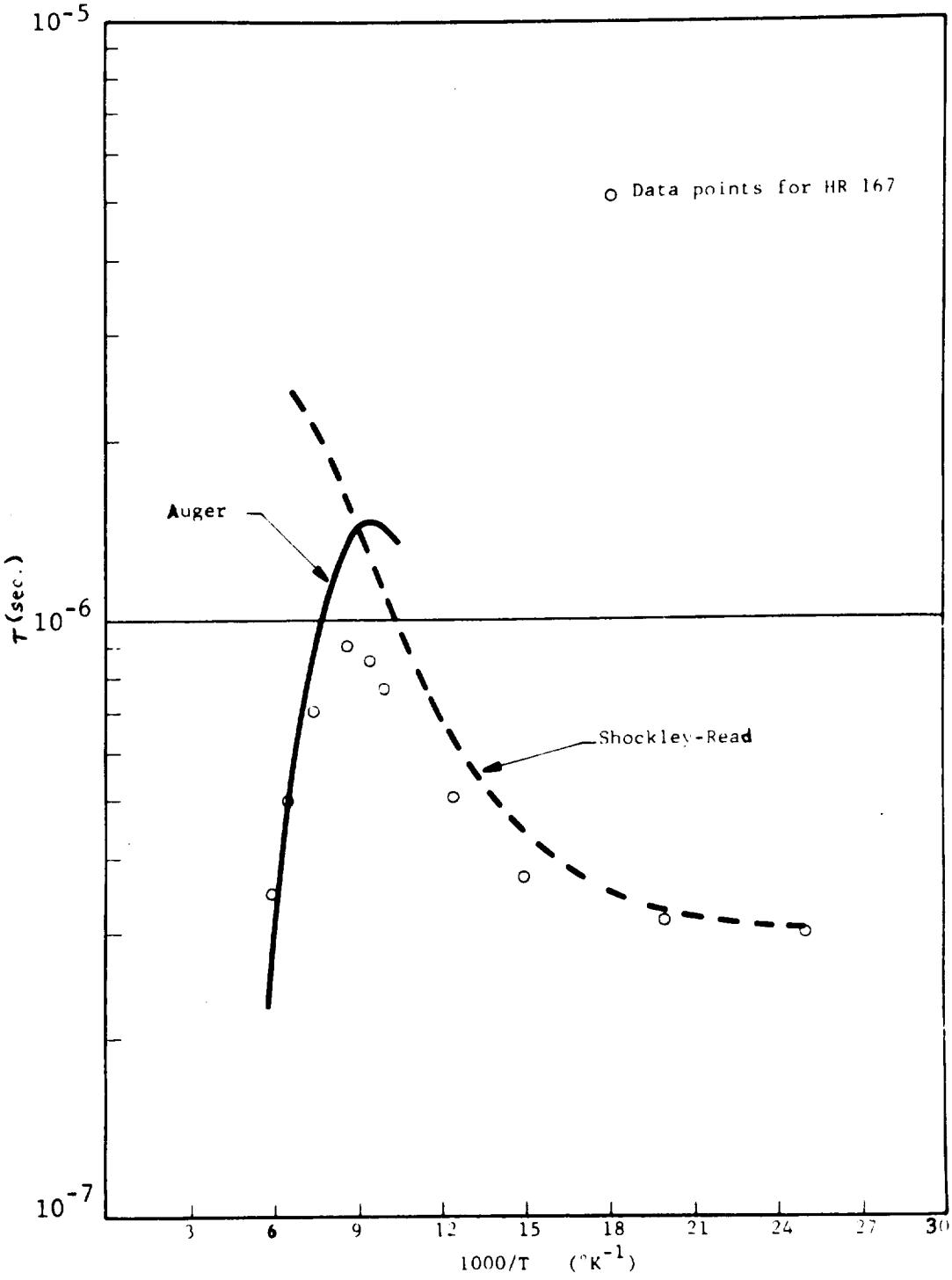

Figure 2.5 THEORETICAL AND ACTUAL LIFETIME AS A FUNCTION OF 100 O/T

Thus, the minority carrier (hole) lifetime in lightly doped n-type material in thermal equilibrium is in the 0.5 to 1 microsecond range in the 77 to 140 °K temperature range. The behavior of the minority carrier (electron) lifetime in p-type material is not as well understood. The Auger lifetime in heavily doped p-type material should be roughly 1 nanosecond in this temperature range.

2.6 HALL COEFFICIENT AND RESISTIVITY

The temperature dependences of the Hall coefficient and resistivity for typical n-type and p-type (Hg,Cd)Te are shown in Figures 2.6 and 2.7. These measurements were made with a continuously recording ac Hall and resistivity system developed by W. Scott and checked at 300 and 77 °K with the standard dc system. The Hall coefficient and resistivity in Figure 2.6 increases monotomically with reciprocal temperature as expected for a "classical" n-type semiconductor. The Hall coefficient calculated from the intrinsic carrier concentration roughly follows the measured Hall coefficient, except at low temperatures where the material becomes extrinsic. This material has been used in the study of p-type diffusions in (Hg,Cd)Te.

The Hall coefficient in Figure 2.7 exhibits a crossover from negative to positive at roughly 135 °K. This is expected in "classical" low energy gap p-type material where $N_A > N_D$. The Hall coefficient and resistivity for a two carrier semiconductor are given by

$$R_H = \frac{-(nb^2-p)}{q\ (nb + p)^2} \tag{2.7}$$

$$\rho = \frac{1}{q\ \mu_p\ (nb + p)} \tag{2.8}$$

where $b = \mu_n/\mu_p$ is the mobility ratio. If $p \sim N_A > N_D$, at temperatures where the material is intrinsic, $n_i b^2$ is greater than p; and the Hall coefficient is negative. At lower temperatures where the material is extrinsic, p is greater than n_b^2, and the Hall coefficient is positive. The small change in resistivity

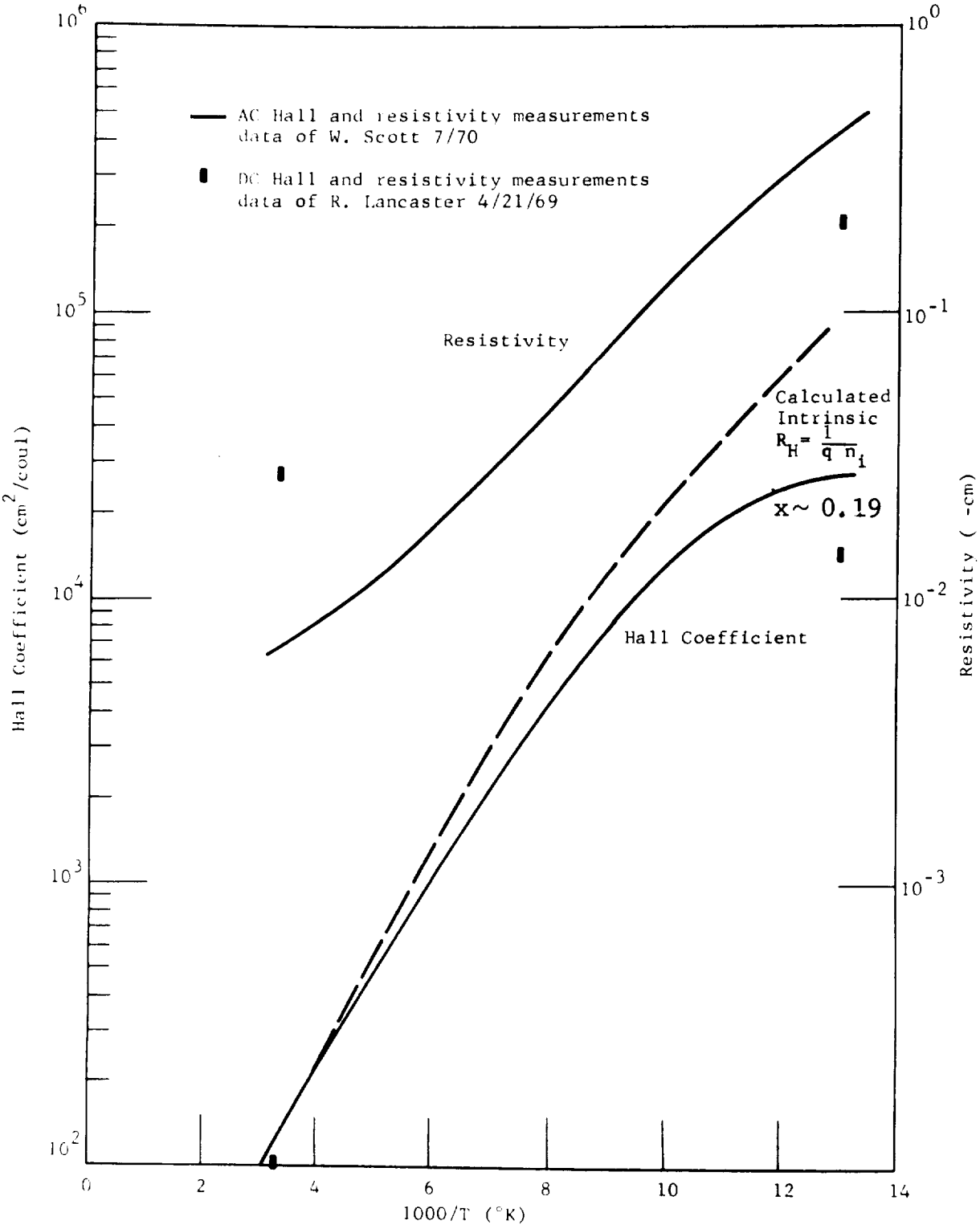

Figure 2.6 "CLASSICAL" N-TYPE (Hg,Cd)Te

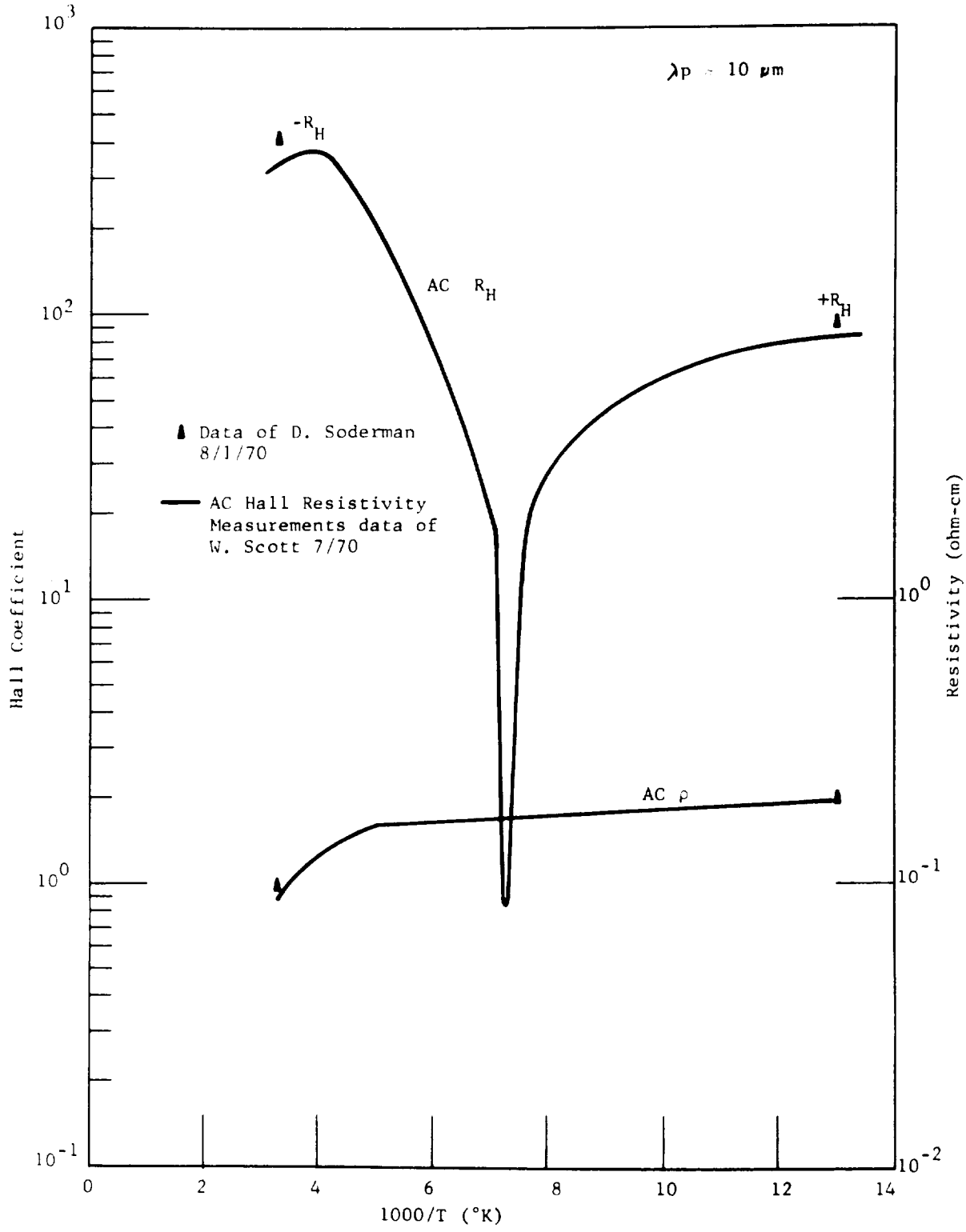

Figure 2.7 "CLASSICAL" P-TYPE (Hg,Cd)Te

can be explained by postulating that the material is essentially p-type ($p > n$) at all temperatures, except that at high temperatures the currents carried by the minority and majority carriers are comparable due to the large mobility ratio b. This material has been used in the study of n-type diffusions in (Hg,Cd)Te.

2.7 MATERIAL SELECTION

Both n- and p-type (Hg,Cd)Te materials as previously described have been selected for diffused p-n junction investigation. Material exhibiting "anomalous" electrical properties which possibly are p-type with an n-type surface inversion[12] layer has been avoided. Thus, n- and p-type material with the following measured and assumed material parameters for 77°K temperature operation has been considered in the design of a high speed 10.6-μm detector.

Parameter	Symbol	Magnitude
(Hg,Cd)Te Composition	x	0.19 to 0.20
Energy Gap	Eg	$\approx$ 0.1 eV
Optical Absorption Coefficient	x	$\approx 2 \times 10^{3}$ cm^{-1}
Electron Effective Mass	m_e^*/m_o	$\approx$ 0.008
Hole Effective Mass	m_h^*/m_o	$\approx$ 0.3
Intrinsic Carrier Concentration	n_i	5×10^{13} cm^{-3}
Electron Mobility	μ_n	2×10^{5} cm^{2} volt^{-1}s^{-1}
Hole Mobility	μ_p	2×10^{2} cm^{2}volt^{-1}s^{-1}
n-type Material		
Donor Concentration	N_D	5×10^{14} cm^{-3}
Lifetime	τ_p	10^{-6} s
p-type Material		
Acceptor Concentration	N_A	10^{16} cm^{-3}
Lifetime	τ_n	10^{-9} s

SECTION 3

JUNCTION FORMATION

3.1 INTRODUCTION

Essential to the fabrication of (Hg,Cd)Te photodiodes is the ability to selectively dope the material and form p-n junctions. The electrical properties of (Hg,Cd)Te can be altered by changing the stoichiometry or by foreign impurity doping. Honeywell has pursued both approaches in junction formation required for photodiode fabrication. Although not a great deal is known about the properties of impurities in (Hg,Cd)Te, it is generally assumed that interstitial Hg and Cd produce n-type conductivity while Hg and Cd vacancies as well as Te interstitials produce p-type conductivity. The adjustment of stoichiometry has been used previously for junction fabrication.

In the present program, mercury in and out diffusion in (Hg,Cd)Te was also investigated. However, it was initially believed that a more stable junction could be produced by impurity diffusion than by deviations from stoichiometry.

One difficulty which has not yet been resolved is the unsuitability of present techniques for determining junction depth of diffused layers. The present thermoelectric probe technique can be in substantial error due to the difference in hole and electron mobilities. Since the hole mobility is less than one tenth of the electron mobility and the intrinsic carrier concentration in the $x \sim 0.20$ composition of (Hg,Cd)Te is comparable to the doping levels, lightly doped p-type material can thermoelectrically probe n-type. Thus, an optical junction measurement technique was attempted in which a beveled surface containing the p-n junction is scanned with a light spot one mil or less in diameter. The photovoltaic signal generated by the spot is measured as the spot traverses the surface. The point at which the signal is a maximum is taken to be the junction location. This technique has been used successfully in higher energy gap material ($x \approx 40$ to 60%), however, in the $x \approx 20\%$ material, a weak signal was generated only in the vicinity of the contacts in the one sample tested. Thus, thermoelectric probing

and diode fabrication are the best available procedures to determine the junction depth.

A useful characterization of a diffusion process requires knowledge of diffused layer conductivity as well as of junction depth. The Van der Paw technique, a four-contact method for measuring resistivity of layers of arbitrary shape, has been used to evaluate several diffusion experiments. The technique is nondestructive and can also be used to measure the Hall coefficient.

3.2 IMPURITY DIFFUSION

3.2.1 Influence of Impurities on the Electrical Properties

There is a large variation of possible dopants which can be used to dope (Hg,Cd)Te. One would expect that elements from columns I and V of the periodic table could act as acceptors by substitution for the cations and anions, respectively, in the crystal lattice, and that elements from columns III and VII could act as donors by similar substitution. However, a few additional requirements have to be considered before we can use a particular impurity.

An important requirement is that the impurity should be able to be diffused into the material at a reasonably low temperature. This is necessary to prevent excessive dissociation of the HgTe and drastically changing stoichiometry. The relatively small dissociation energy of HgTe greatly complicates the diffusion and annealing procedures for junction preparation. A second problem encountered and also due to the small dissociation energy of HgTe, is the tendency of the impurity atom to displace the Hg from the lattice and form yet another compound rather than dope the crystal. Examples of this are In_2Te_3, TeI_2 and TeI_4.

We have observed that when copper and gold (from column IB) are diffused into n-type (Hg,Cd)Te, the (Hg,Cd)Te thermoelectrically probes p-type at low temperatures in the vicinity of 100°K, which indicates that copper and gold behave as acceptor states. These effects are not simply the result of a mercury out-diffusion (deviation from stoichiometry), since the unplated, undiffused areas of (Hg,Cd)Te remained n-type after the impurity diffusion.

Radioactive tracer measurements have confirmed the high gold concentration in the diffused layers.

It is difficult to evaluate the electrical properties of the high resistance p-type diffused layer on the low resistance base material. However, the sheet resistance measured between contacts on the gold diffused layer of a mesa diode (10968 S-117G) is between 45 and 90 ohms at 77 °K, while the resistance decreases to roughly 4 ohms at 300 °K. At both temperatures the current-voltage characteristics are linear indicating ohmic conduction. Similar sheet resistances at 77 °K are calculated assuming an average acceptor concentration 10^{17} cm^{-3}, 3-μm junction depth, and hole mobility 200 cm^2/volt-s.However, at higher temperatures, the shunt conductance of the n-type base material becomes dominant. The high sheet resistance at low temperatures results in a high series resistance in the diode which is apparent in the diode current-voltage characteristics.

An alternate approach yielding photodiodes with a lower series resistance consists of diffusing a donor impurity into p-type material. Thus, a bromine diffusion investigation was initiated. Bromine was chosen because it should diffuse into (Hg,Cd)Te material in the presence of a high mercury vapor pressure and substitutionally replace the tellurium resulting in a donor impurity level. The high mercury vapor pressure is required to suppress mercury vacancy formation which results in acceptor states. P-type samples from ingot 20769 and 6-470 were sealed in several evacuated quartz tubes with a mixture of prereacted bromine and mercury. One tube was diffused for 17 hours at 275°C, another for 2 weeks at 275 °C, and the last left at room temperature for several weeks. A nonconducting (greenish) layer formed on all the surfaces of the samples. When this layer was lapped away, the material thermoelectrically probed p-type at 77 °K as before diffusion. The formation of a bromine compound on the surface probably inhibited the diffusion of bromine into the material and, thus bromine diffusion into (Hg,Cd)Te by this technique does not appear promising.

3.2.2 Radioactive Gold Tracer Study

In the investigation of p-n junction formation by gold diffusion, the question has arisen whether the diffused p-type region is the result of a gold acceptor state or a mercury vacancy. It is known that the electrical conductivity type in (Hg,Cd)Te can be altered by heating the sample under various mercury vapor pressures.

In our recent investigation of p-n junctions in (Hg,Cd)Te, we have found that junctions can be fabricated by plating the surface with gold and then giving the sample a low temperature (250 - 300 °C) heat treatment. W. Scott has shown that the junction depth substantially decreases when the samples are given a heat treatment in the presence of a high mercury vapor pressure. Thus, one may assume that this diffusion mechanism involved the movement of mercury vacancies. However, it has never been established that the gold actually diffuses into the (Hg,Cd)Te and does not act as a "sink" for excess mercury which may out diffuse. Gold readily forms an amalgam with free mercury and this is apparent with the discoloration of the gold layer in the vicinity of a mercury pit. Thus, a radioactive gold tracer study was initiated to establish that the gold actually does diffuse into the (Hg,Cd)Te. The results of this study show that gold does diffuse into the (Hg,Cd)Te however, it is in much higher concentrations than previously assumed, and its concentration profile indicates the presence of two diffusion mechanisms.

These radioactive tracer measurements were made as part of an ID/AR program with the assistance of H. Carter at Tracerlabs (LFE Corporation, Waltham, Massachusetts). Radioactive gold (atomic weight 199, half life 3.15 days) was selected because it could be supplied carrier free (less than 2% stable gold) in a gold chloride solution. Radioactive gold was plated on the top surface of a small sample of $(Hg_{0.8},Cd_{0.2})Te$ material adjacent to that previously used for gold diffusion studies. The sample was given a typical heat treatment which has yielded p-n junctions in 7-μm (Hg,Cd)Te. The remaining radioactivity in counts/minute was measured as material and lapped away from the diffusion surface. The gold concentration profile was calculated from the specific activity and the change in radioactivity as material was removed from the surface. Figure 3.1 shows the calculated gold concentration and the conductivity type as measured using a thermoelectric probe.

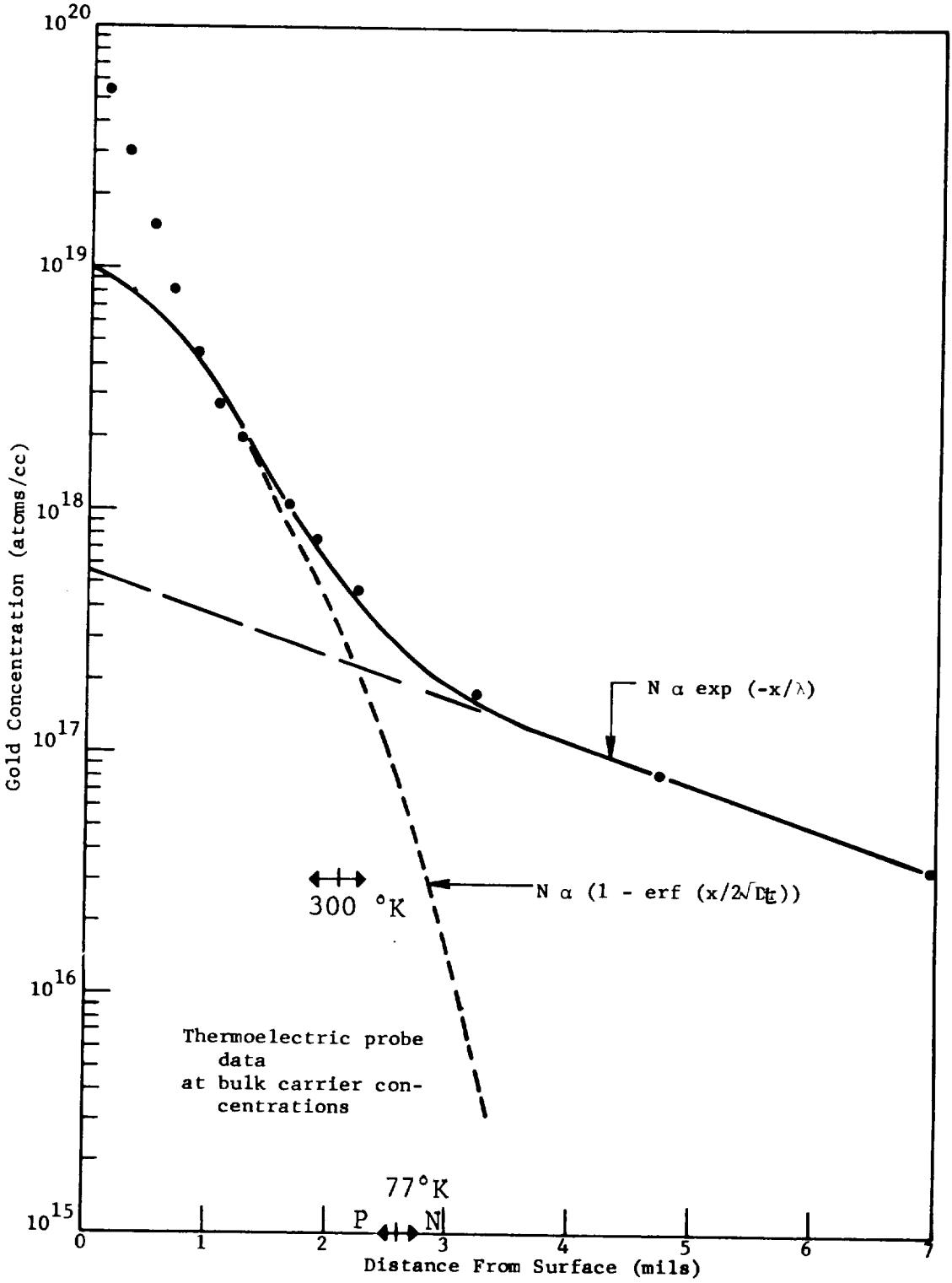

Figure 3.1 GOLD CONCENTRATION VS DISTANCE $(Hg_{0.2},Cd_{0.8})Te$

These radioactive tracer measurements are probably accurate to within a factor of two of the actual average gold concentration. However, this technique measures the gold which may have segregated out at dislocations and crystal defects as well as the electrically active gold distributed through the sample. The (Hg,Cd)Te samples had no apparent grain boundaries and a very low density of mercury pits; however, it is possible that a substantial amount of gold has segregated out at these defects and has increased the apparent gold concentration. After the gold deposition and diffusion, the surface is pitted with excess gold which is not soluble in the material and results in a very large apparent surface concentration.

As shown in Figure 3.1, the gold diffuses via two diffusion mechanisms. This fast and slow cation diffusion has been observed in other II-VI semiconductors. The fast diffusion component can best be described by an exponential profile

$$N \alpha \exp(-x/\lambda) \tag{3.1}$$

which is similar to the diffusion along dislocation observed by Whelan and Shaw[14] in the self diffusion of cadmium in cadmium telluride and by Nebauer[15] in gold diffusion in cadmium sulfide. The slow diffusion component can be fitted to a complementary error function distribution expected from Fick's law.

$$N \alpha 1 - \mathrm{erf}[(x/2\sqrt{Dt})] \tag{3.2}$$

with a diffusion constant $D \approx 5 \times 10^{-10}$ cm^2/s at 275 °C.

The addition of these two diffusion components yields a profile which is in good agreement with that measured for $x > 1$ mil.

The slow diffusion component observed in gold diffused (Hg,Cd)Te is believed to be substitutional gold replacement of mercury resulting in an electrically active acceptor dopant. This is supported by the thermoelectric conductivity data. Assuming a reasonable mobility ratio (10-100), this thermoelectric data is consistent with the slow diffusion profile. Also, the junction depth shown in Figure 3.2 roughly follows a square root time dependence as

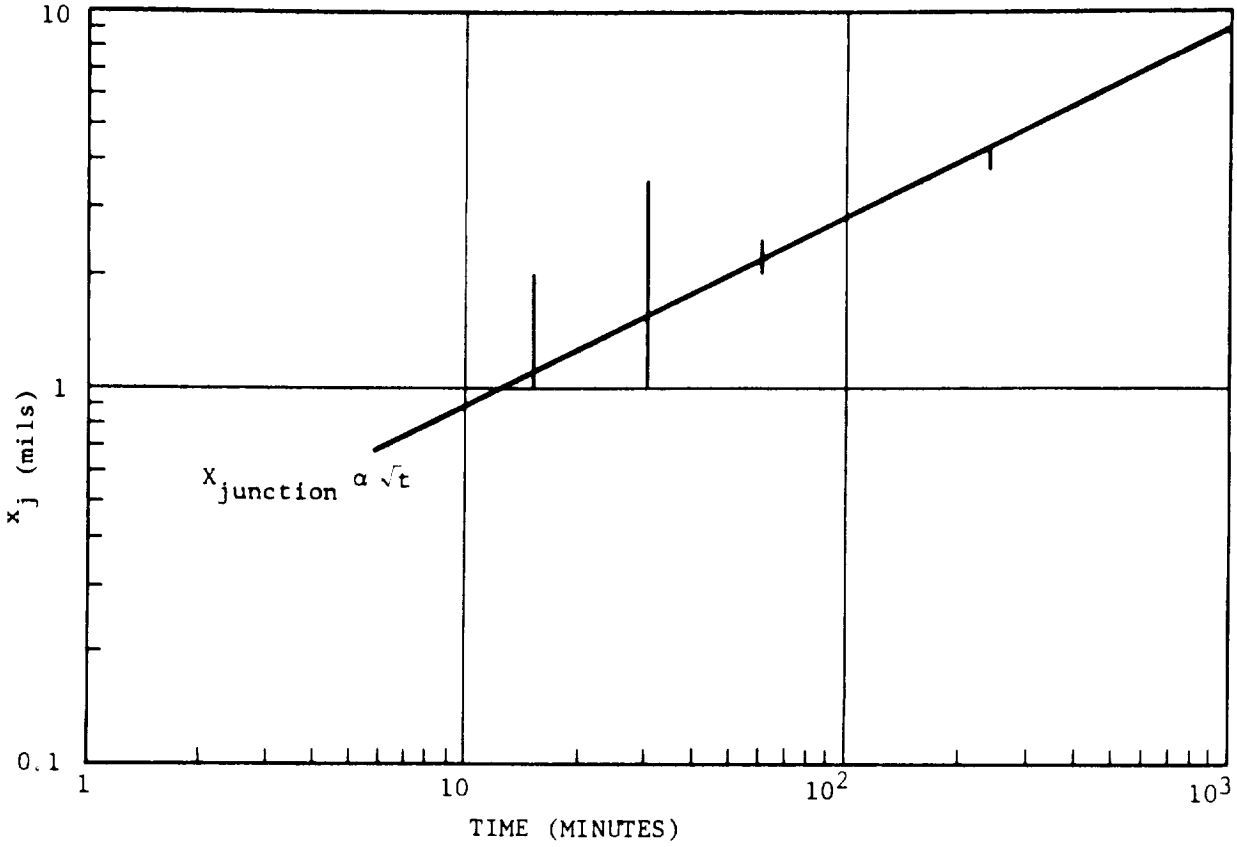

Figure 3.2 JUNCTION DEPTH VS GOLD DIFFUSION TIME IN $(Hg_{0.2},Cd_{0.8})Te$ (JUNCTION DEPTH MEASURED BY THERMAL PROBING AT 77 °K)

expected from Equation 3.2. Thus, the slow substitutional diffusion component is believed to be electrically active as opposed to the fast interstitial diffusion component.

3.3 DEVIATIONS FROM STOICHIOMETRY

P-n junctions can be prepared by a nonstoichiometric condition via mercury in and out-diffusion. The samples are sealed in an evacuated quartz tube with a few grams of mercury. The in and out-diffusion of mercury can be adjusted by varying the temperature of the mercury and, hence the mercury vapor pressure in the tube. All the mercury diffusions have been performed with the (Hg,Cd)Te samples between 250 and 300 °C. It should be noted that not all p-type (Hg,Cd)Te material can be converted to n-type via this mercury anneal, however, all n-type can be made p-type with the formation of mercury vacancies.

3.3.1 Mercury In-Diffusion

The initial mercury in-diffusion experiments were performed with a large mercury vapor pressure. However, the resulting p-n junctions exhibited no reverse bias saturation currents and large capacitances as expected for heavily doped p- and n regions. The basic approach in avoiding tunnel currents in 10.6-μm (Hg,Cd)Te junctions is to reduce the carrier concentration in the p-type side of the junction.

Two factors complicate this problem. First, the hole concentration in the starting material is controlled only within rather broad limits owing to the nature of the fabrication process. Second, the diffusion process involves an elevated temperature treatment, which can be expected to generate mercury vacancies that behave as electrically active acceptor states. Accordingly, a program of elevated temperature mercury diffusions was planned and carried out.

It was desired to investigate the effect of various mercury diffusion treatments on both conductivity types of material which are affected by the diffusion. Three n-type and three p-type samples were used. Resistivity was measured before and after diffusion. Hall coefficient measurements were previously made on samples taken from the same ingots as the samples used in this study. The Hall coefficient was measured on each of the six diffused samples after diffusion. Finally, on the samples which were initially

p-type, the approximate depth of the n-region after diffusion was determined by thermal probing. Mesa-type diode structures were fabricated from two of the p-type samples, and were evaluated.

Three elevated temperature treatments were used. All samples were subjected to an initial brief diffusion with a high mercury vapor pressure which should saturate the sample surface with mercury, and defects (mercury vacancies) would be formed in the interior. The first group of samples quenched to room temperature should retain the defects. The second group of samples was given a longer diffusion with a reduced mercury vapor pressure which should result in the surface mercury diffusing further into the material. Quenching after this treatment should "freeze-in" the defects formed by the high temperature. The third group of samples was given a slow cooldown to room temperature after the initial mercury diffusion. This slow cooldown would be expected to permit defects to anneal without causing further mercury diffusion. One n-type and p-type sample was given each treatment.

The resistivity before and after diffusion of the three n-type samples is shown in Figure 3.3. The resistivities of the three samples prior to diffusion was not characteristic of classical n-type (Hg,Cd)Te. None of the three treatments substantially changed the apparent resistivity of the materials, with the exception of second treatment[2].

The Hall coefficients of the same samples are shown in Figure 3.4. Here the difference between the two quenched samples is insignificant below room temperature. Also, all annealing treatments lowered the Hall coefficient by over an order of magnitude. The dependence of R_H on temperature in the range from 140 °K to 300 °K is similar to the dependence for the undiffused sample. The less abrupt spectral cutoff wavelength of these samples indicates that the mercury has had a significant effect on the (Hg,Cd)Te surface composition and energy gap.

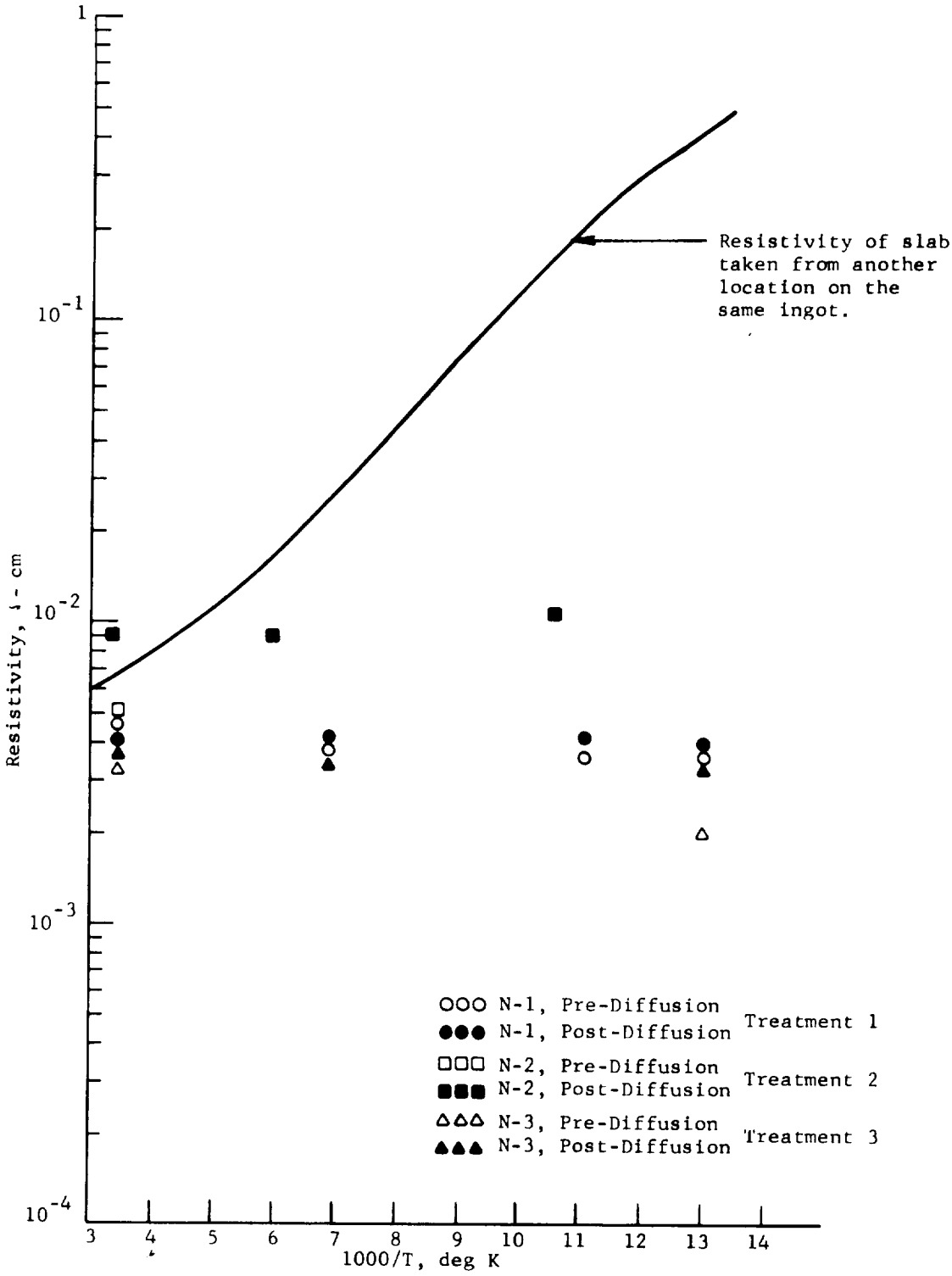

Figure 3.3 EFFECT OF HIGH TEMPERATURE TREATMENT ON N-TYPE SAMPLE CONDUCTOR

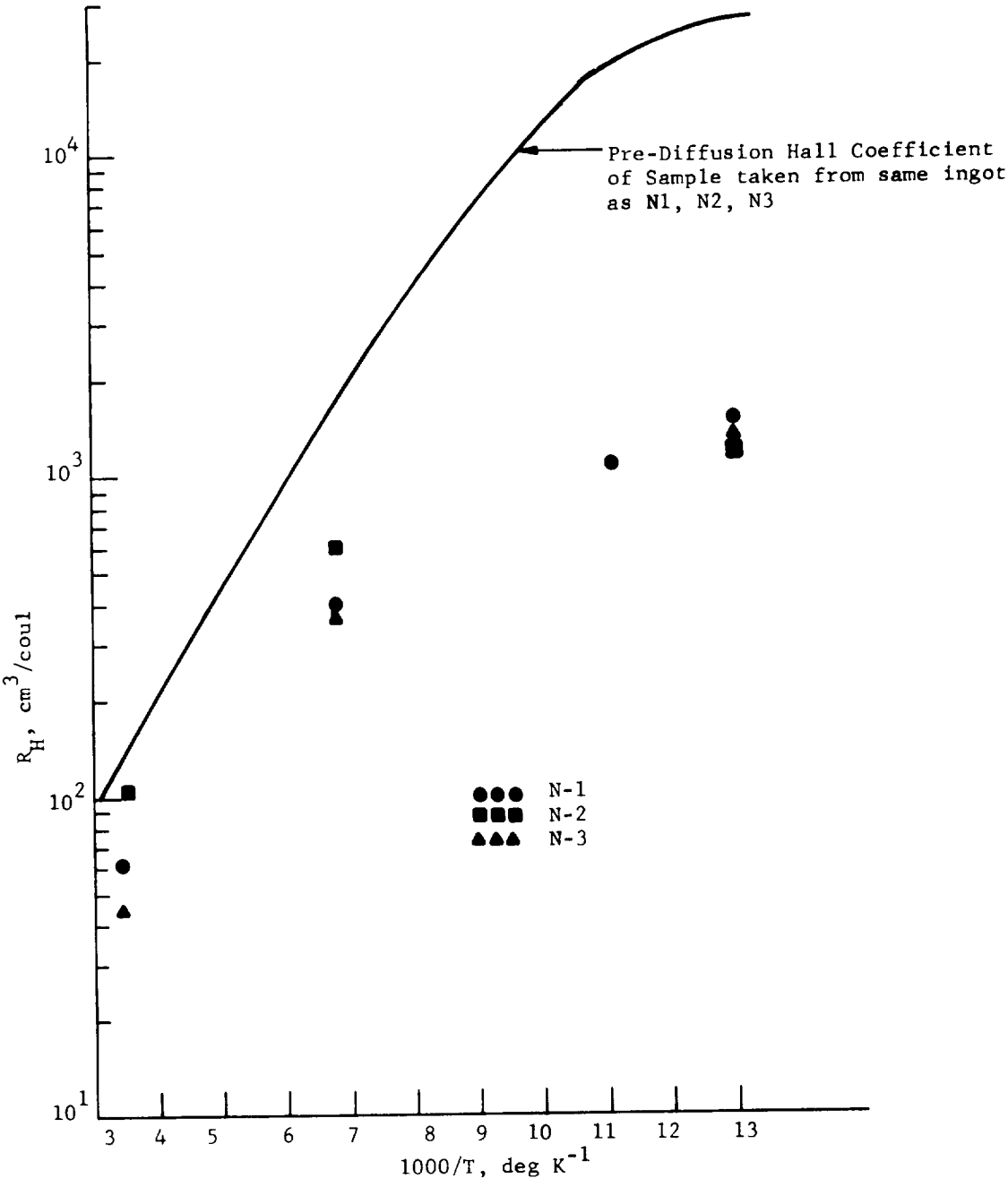

Figure 3.4 EFFECT OF TEMPERATURE TREATMENTS ON N-TYPE HALL COEFFICIENT

Figure 3.5 shows resistivities of the three p-type samples before and after diffusion. The shapes of the curves are similar for all six cases. It should be recalled that the post diffusion data presumably refers to the n-diffused layer only, and were calculated on that basis.

The fact that the diffused layer resistivities do not show the temperature dependence expected from n-type material is under investigation. It is believed that either the layers are degenerate or that the measurement is being dominated by the base, p-type, region.

Figure 3.6 shows the Hall coefficients of the p-type samples after diffusion. The data for P2 and P3 are suggestive of n-type material in shape. The data for P1, which had only a 30-minute treatment, indicates that the surface of P1 may still be p-type. If the measurement could have been made at lower temperatures, it is believed the curve for P1 would have shown the dip characteristic of the Hall coefficient of p-type material.

3.3.2 Mercury Out-Diffusion

It is possible to convert the surface of n-type material to p-type by introducing mercury vacancies which are known to behave as acceptors. We propose to use this phenomenon to produce p on n-type photodiodes, which theoretically should have a faster response time than n on p-type due to the higher electron minority carrier mobility. The objective of this study is to investigate the diffusion times and temperatures which result in a consistent and reproducibile method of shallow p-n junction fabrication.

An initial experiment with mercury out-diffusion consisted of heating the surface of a (Hg,Cd)Te sample to 200 °C by focusing an intense beam of light onto the slab. It was expected that most of the light absorption would take place at the surface, thereby causing the excess mercury at the surface to evaporate. The first sample on which this technique was tried showed a p-type surface at 77 °K immediately after the heating. After several minutes, however, the surface had reverted back to n-type. The reason for this change is not known, but further experiments with this technique are planned.

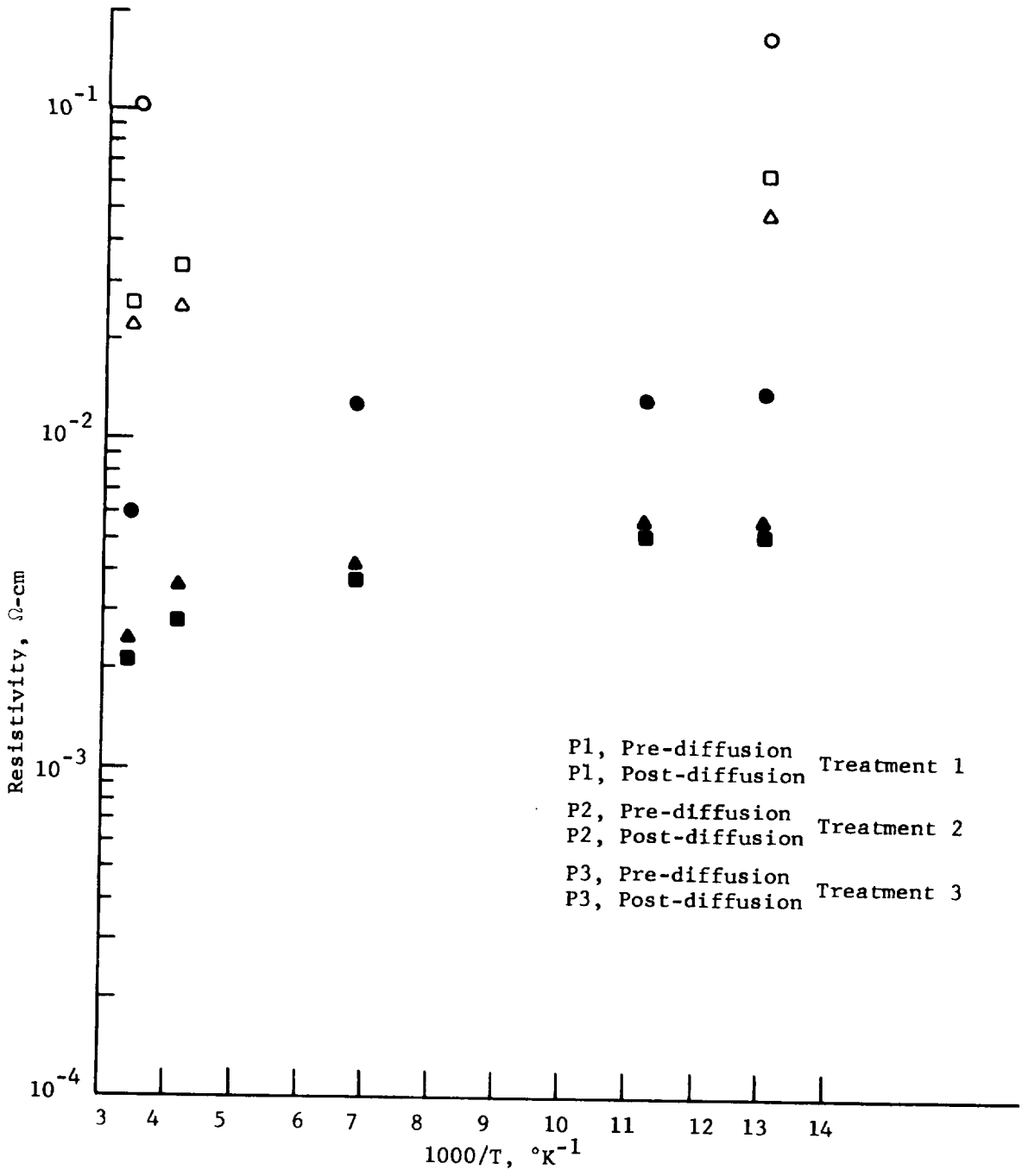

Figure 3.5 EFFECT OF HIGH TEMPERATURE MERCURY TREATMENT ON RESISTIVITIES OF P-TYPE SAMPLES

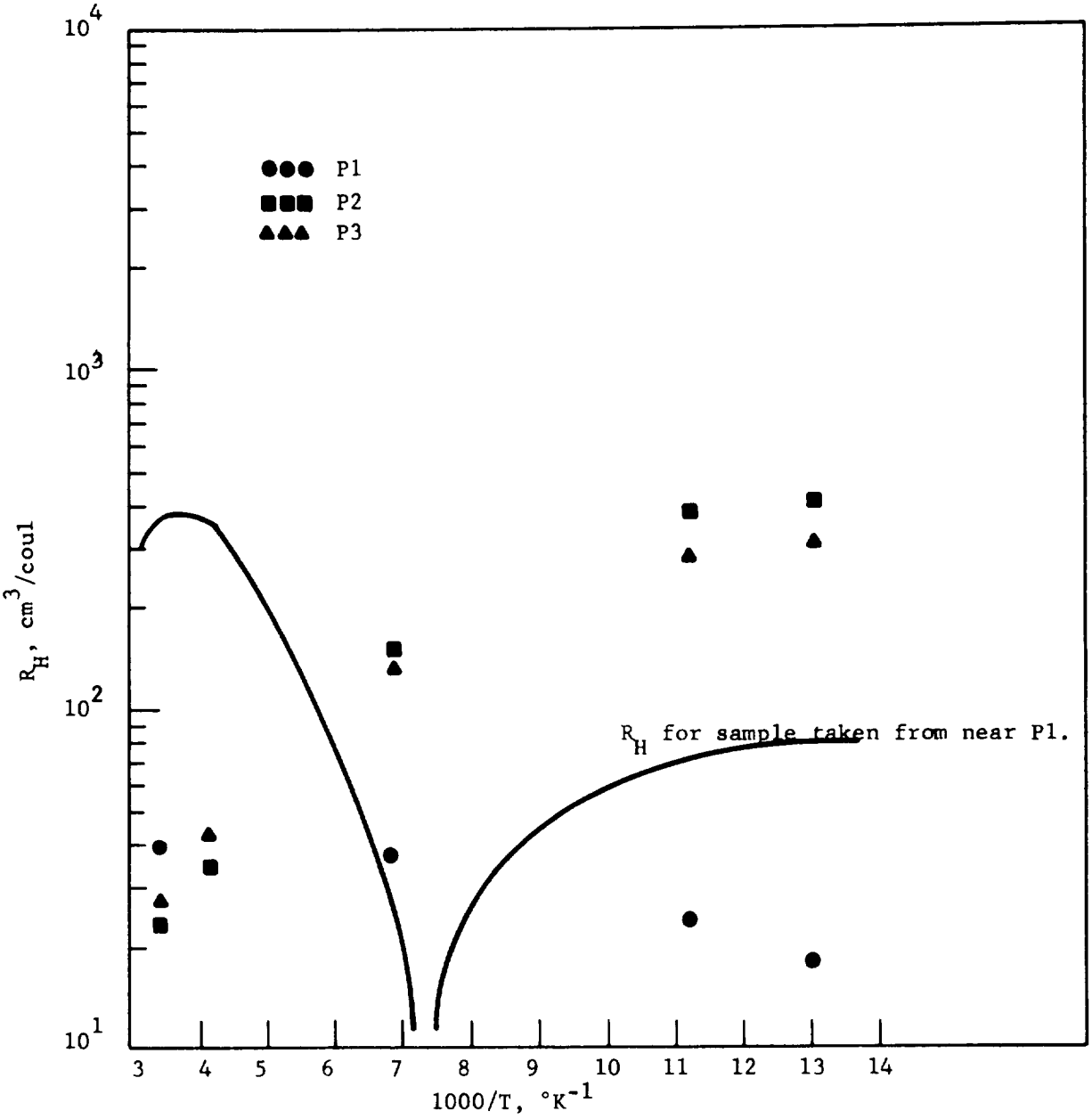

Figure 3.6 EFFECT ON ELEVATED TEMPERATURE MERCURY ANNEAL ON HALL COEFFICIENT OF P-TYPE SAMPLES

SECTION 4

PHOTODIODE DESIGN CONSIDERATIONS

The development of a photodiode having the desired responsivity, response time, and quantum efficiency will require a successful combination of design, material properties, and fabrication procedures. Previous sections of this report have shown how the properties of (Hg,Cd)Te alloys vary with composition, doping, temperature, and diffusion parameters. In this section, the photodiode design and performance based on material properties are discussed. After a general description of a photodiode and its mode of operation, the p-n junction characteristics, response time, and sensitivity performance are discussed.

4.1 INTRODUCTION

Photons which have the proper energy to be absorbed in the region of a p-n junction, produce an output potential across the junction caused by the diffusion of photoexcited electrons and holes. Figure 4.1 shows the physical configuration of such a photodiode. The diode has three electrically different regions: p-type, n-type and the depletion region. In this particular model the infrared radiation is incident on the n-type layer. Electrical contacts are made to the n- and p-type regions. The output signal of such a device is proportional to the amplitude modulation of the infrared radiation.

The Fermi levels in p- and n-type regions are aligned in the absence of radiation to balance the diffusion of electrons and holes from each side of the junction. The resulting electric field in the depletion region accelerates any mobile carriers out of the depletion region. Because the minority carriers diffuse across the junction, their densities are reduced within a diffusion length L of the depletion region. The distribution of the photoexcited electron hole pairs created in these three regions depends on the absorption coefficient of the semiconducting material which is a function of the radiation wavelength (photon energy). Ideally, all the electron-hole pairs are created within the depletion layer. Then the internal electric field splits the pair, moving the hole into the p-type material and the electron

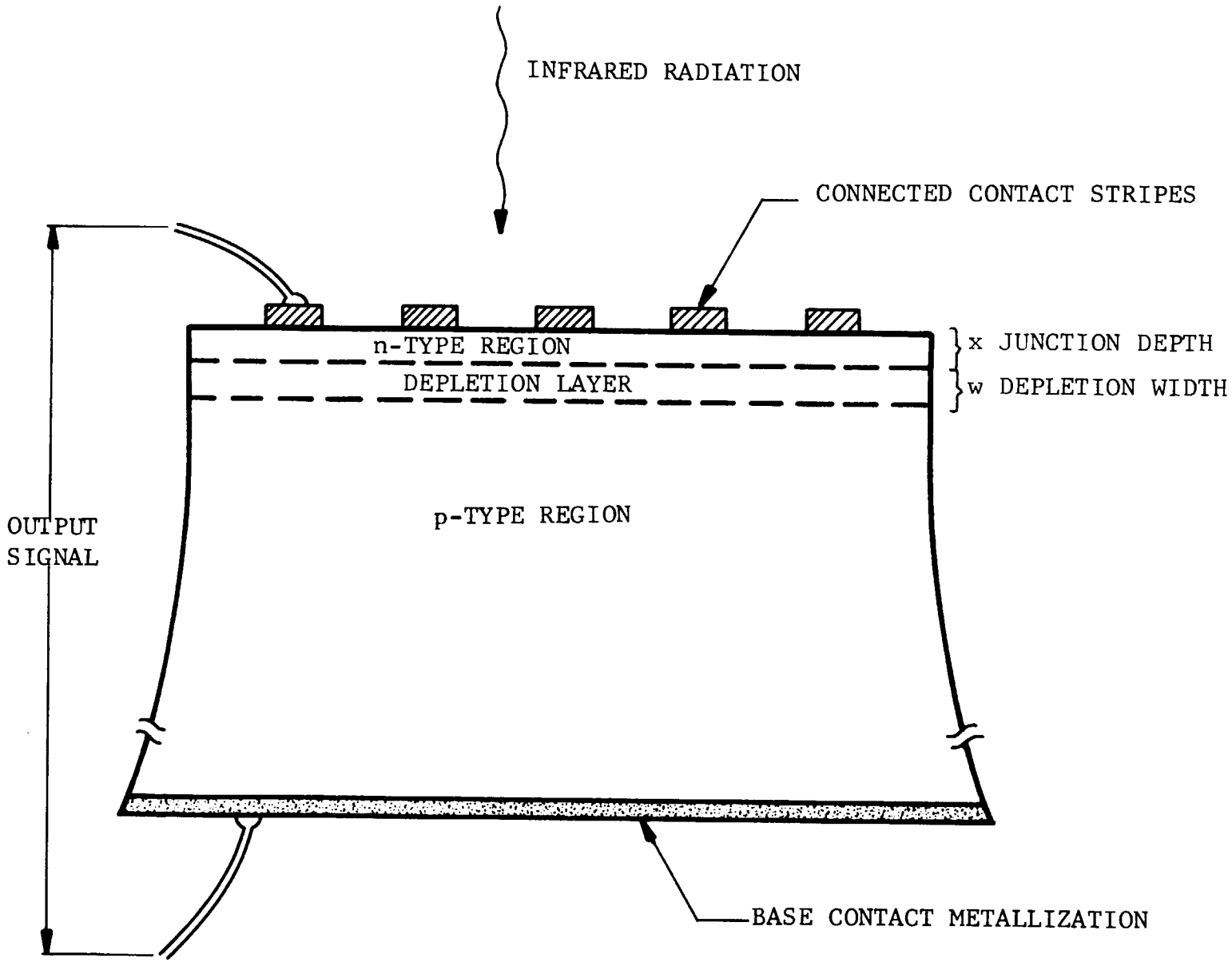

Figure 4.1 PHYSICAL CONFIGURATION OF A PHOTODIODE

into the n-type material, contributing to the signal current. In a practical situation there are always some photoexcited carriers generated on either side of the depletion layer. In this case, only the excess minority carriers diffuse across the junction and contribute to the signal current. The movement of electrons and holes causes the n-type material to be charged negatively and the p-type material to be charged positively. An open circuit voltage will then be generated across the detector, and if a load resistor is connected across the device, a current will flow.

The photodiode can also be operated with a dc reverse bias voltage. This externally applied voltage increases the depletion region, thereby increasing the number of photoexcited electron hole pairs generated within the depletion region. In this mode of operation the amplitude modulation of the infrared radiation is proportional to the ac short circuit signal current. This reverse bias mode extends the frequency response of the photodiodes and is better matched to broadband preamplifiers.

At large reverse bias voltages near the avalanche breakdown voltage, photoexcited electrons and holes traversing the depletion layer gain enough kinetic energy to impact ionize bound charges. Each collision produces secondary carriers which may also create other electron hole pairs giving rise to a gain mechanism. Such an avalanche gain is extremely important in increasing the detector-preamplifier detection preformance since the broad band preamplifier noise usually dominates the detector noise. Thus, the signal and detector noise can be amplified by the avalanche gain mechanism, increasing the performance until the detector noise becomes comparable to that of the preamplifier.

4.2 P-N JUNCTION CHARACTERISTICS

The dc current-voltage (I-V) characteristics for a simple one dimensional model of p-n junction is given by

$$I = \begin{cases} I_o \left(e^{qV/KT}-1\right) + I_{gr} \dfrac{\sinh\left(qV/2KT\right)}{q(V_D-V)/KT} & V>0 \\ I_o + GV + I_p + I_{gr} & V<0 \end{cases} \qquad (4.1)$$

where

I_o = diffusion limited saturation current

$$= Aq\left(\frac{D_p p_n}{L_p} + \frac{D_n n_p}{L_n}\right)$$

GV = surface leakage

I_p = current induced by absorption of radiation

I_{gr} = space charge generation recombination current

$$\approx \frac{Aqn_i W}{\sqrt{T_{po} T_{no}}}$$

assuming recombination centers midway in the energy gap, see References 16 and 17.

A = junction area

D_p, D_n = diffusion constant for holes and electrons

$$= \frac{\mu_{p,n} KT}{q}$$

L_p, L_n = diffusion length for holes and electrons

$$= \sqrt{D_{p,n} \tau_{p,n}}$$

p_n, n_p = hole and electron minority carrier densities

n_i = intrinsic carrier concentration

$\tau_{p,n}$ = hole and electron minority carrier lifetimes

W = depletion layer width

The diffusion and space charge generation reverse bias currents have been calculated for a p-n junction in $(Hg_{0.81}Cd_{0.19})$ Te material assuming the measured and calculated material parameters discussed in Section 3 and listed in Table 4.1. Over the 77 to 140°K temperature range, the Auger lifetime has a slow variation and for these calculations can be considered temperature independent. The temperature dependences of the diffusion and space charge generation currents for a 1μm depletion layer are shown in Figure 4.2. At low temperatures the diffusion and space charge generation currents are comparable, but as the temperature is increased, the diffusion current, which varies as n_i^2 as opposed to the n_i dependence of the space charge, becomes dominant. Also shown is the current induced by the absorption of 300°K background radiation assuming a 60°FOV and 0.2 quantum efficiency. Thus, at low temperatures the photodiode performance can be increased by limiting the field of view.

A small signal equivalent circuit for a diode is shown in Figure 4.15 The shunt resistance R_d and depletion capacitance C_d both vary with the dc operating point. The low frequency ($\omega\tau < 1$) small signal shunt resistance at 77°K and zero bias is given by

$$R_d = \frac{\beta\ kT}{q\ I_o} \qquad (4.2)$$

where $\beta \approx 1$ is the recombination coefficient. Thus a photodiode with a $4 \times 10^{-4} cm^2$ area should have roughly a 500 ohm junction resistance at 77°K.

The junction capacitance is composed of a depletion and diffusion component. Under reverse bias conditions, the depletion capaci-

Table 4.1

MEASURED AND CALCULATED VALUES OF (Hg,Cd)Te PROPERTIES AND PHOTODIODE DIMENSIONS

Property or Dimension		Value	How Determined
	Junction type	abrupt	-
	Area	4×10^{-4} cm^2	-
	Temperature	80°K	-
N_D	donor concentration	5×10^{14} cm^{-3}	Assigned
N_A	acceptor concentration	10^{16} cm^{-3}	Assigned
n_i	intrinsic carrier concentration	4×10^{13} cm^{-3}	Calculated (2.3)
τ_p	minority carrier (hole) lifetime in n-type	10^{-6} s	measured data (2.5)
τ_n	minority carrier (electron) lifetime in p-type	10^{-9} s	extrapolated
μ_n	electron mobility	2×10^5 cm^2 V^{-1} s^{-1}	measured (2.4)
μ_p	hole mobility	2×10^3 cm^2 V^{-1} s^{-1}	approximation based on measurement
L_n	minority carrier (electron) diffusion length in p-type material	10μm	calculated
L_p	minority carrier (hole) diffusion length in n-type material	10 μm	calculated
I	reverse bias current	12×10^{-6} A	calculated (4.2)
R_D	diode resistance	500 ohms	calculated(4.2)
R_s	series resistance	<10 ohms	calculated ref. 14
η	quantum efficiency	0.25	calculated (4.3)
S	sensitivity	2.5 A/watt	calculated (4.3)
C_D	diode capacitance	4 pF	calculated (4.2)

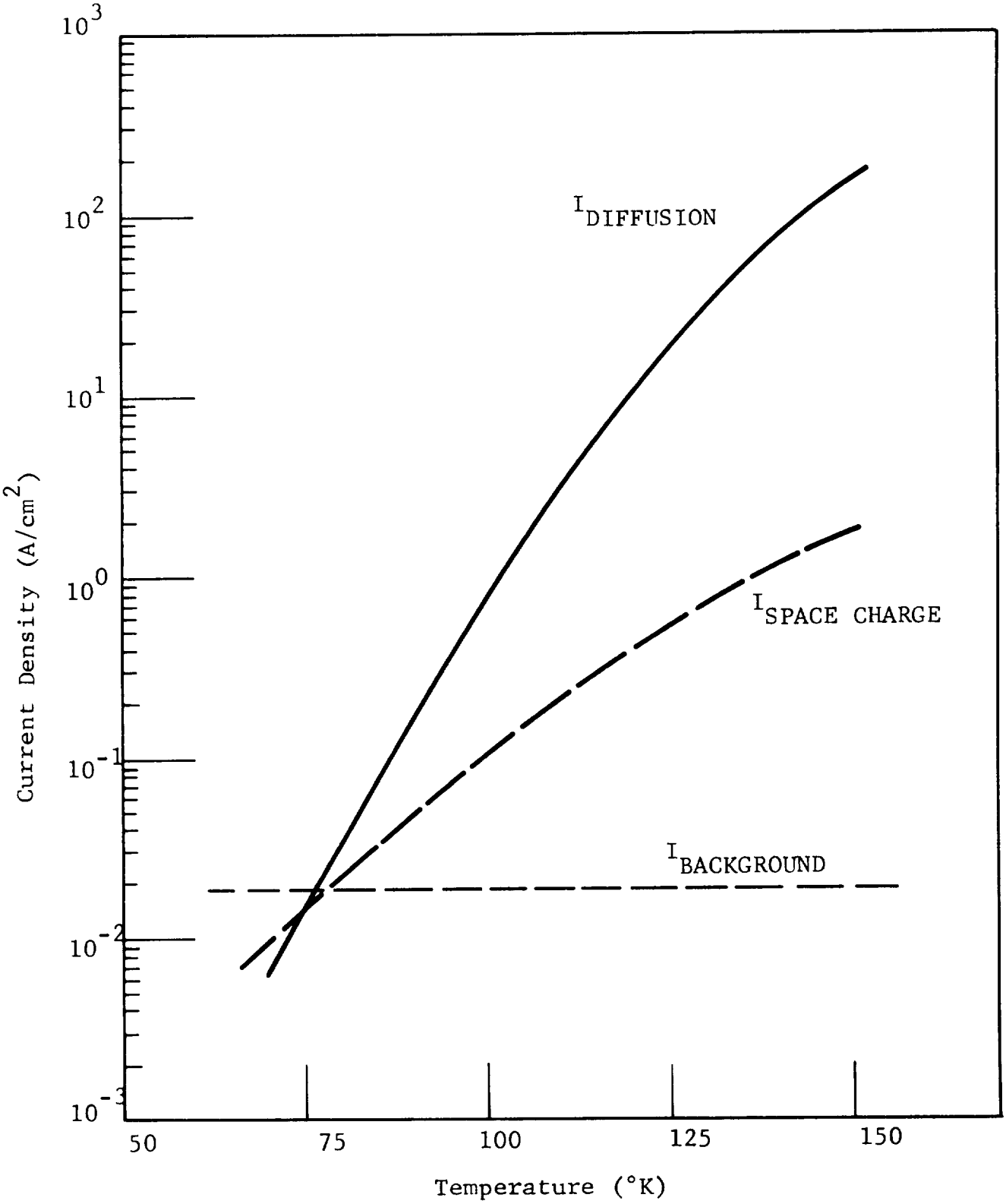

Figure 4.2 CALCULATED REVERSE BIAS CURRENT DENSITY VS TEMPERATURE (ASSUMING MATERIAL PARAMETERS IN TABLE 4.1)

tance is dominant. The depletion capacitance for an abrupt p-n junction is given by

$$C_d = A\sqrt{\frac{q \epsilon N_D N_A}{2(N_D + N_A)(V + \phi)}} \qquad (4.3)$$

where N_A and N_D are the acceptor and donor impurity doping concentration in the respective sides of the junction and ϕ is the contact potential. ϕ should be roughly 0.05 volt with the proposed impurity concentrations. Thus, with a few tenths of a volt reverse bias voltage, the depletion capacitance should be roughly 4 pF.

The series resistance R_s calculated from the bulk resistivity and the contact spreading resistance[11] should be less than 10 ohms.

4.3. SENSITIVITY AND QUANTUM EFFICIENCY

In the design of a sensitive high speed photodiode, there are several parameters which have to be carefully selected to obtain the optimum sensitivity and electrical bandwidth. The junction depth is one of these parameters. The deeper the junction the higher the quantum efficiency and therefore, the greater the sensitivity. However, deeper junctions also have a longer transit time associated with the diffusion of minority carriers to the junction. Thus, if the speed of the photodiode is transit time limited, a deep junction photodiode would be slower than a shallow junction photodiode.

The steady state response of a graded base photodiode has been calculated by Jordan and Milnes[17] by solving the continuity equation in the p-type base region in terms of dimension less parameters αw, sw/D_n, w/L and βw.

$$\frac{\partial n}{\partial t} = \frac{n_p - n}{\tau_n} + \frac{1}{q}\frac{\partial Jn}{\partial x} + g \qquad (4.4)$$

J_n = current density actually caused by electron motion

n_p = equilibrium electron concentration

τ_n = minority carrier (electron) lifetime

α = absorption coefficient

w = junction depth

s = surface recombination velocity

$D_n = L_n^2/T_n$ = electron diffusion coefficient

β = electric field resulting from gradient in doping concentration

g = generation rate due to incident photon flux

The sensitivity (directly related to the external quantum efficiency) and response times are derived from solutions to this equation. The parameter αw may be interpreted as the ratio of base width to the mean depth of penetration $1/\alpha$ of the incident radiation. The parameter sw/D_n and w/L are associated with the minority carrier loss and volume recombination, respectively. The effect of the built-in electric field (βw parameter) is to accelerate minority carriers to the junction, decreasing the transit time.

With a 10-μm junction depth, the built in electric field resulting from the gradient in doping concentration is approximately 10 V/cm. The best estimate of the surface recombination velocity ($s \sim 10^4$cm/s) has been interpreted from the thickness dependence of the n-type photoconductive detector response time[11]. Substituting previously stated diffusion constants for 77°K operation there is a negligible increase in the reverse bias current due to minority carriers generated at the surface being swept across the junction. At the same time a high sensitivity with 40 percent external quantum efficiency including the front surface reflectivity is calculated. In practical situations, there are other factors such as window reflections and non-ideal device

parameters which tend to reduce the quantum efficiency. However, we feel that a 2.5A/W sensitivity and a 25-percent quantum efficiency are readily achievable.

The response time of a photodiode may be limited by either the transit time, recombination time, or the RC product. There is a transit time associated with the motion of minority carriers in the p-type surface layer and in the depletion region. With a 4-μm junction depth, the transit time for electrons to diffuse from the surface to the junction is

$$\tau = (d_j)^2/(\frac{kT}{q}\ \mu_n) \approx 1 \times 10^{-10}\ s \qquad (4.5)$$

In a diffused junction, the graded doping profile will establish an electric field which will reduce this transit time.[17] In either case, the transit time for excess minority carriers in the surface layer is much smaller than the effective lifetime, including surface recombination, so that most of the photoexcited minority carriers will traverse the junction contributing to the signal current rather than recombining.

Also, there is a transit time associated with carriers traversing the depletion region. For large reverse bias, the maximum depletion width x_j is about 2 μm; and this transit time is

$$\tau = x_j/V_e \approx 2 \times 10^{-11}\ s \qquad (4.6)$$

where V_e is the average velocity obtainable for an electron (approximately 10^7 cm/s). This transit time is reduced with lower reverse bias voltage.

Since the absorption is roughly $2 \times 10^3\ cm^{-1}$, less than ten percent of the photoexcited carriers are generated more than 10 μm from the surface. Thus, there are very few excess minority carriers which have to diffuse to the junction from deep within the n-type material, and this transit time can be neglected.

The response time may be limited also by the $R_{eff}C$ product where C is the depletion layer capacitance and R_{eff} is the effective shunt resistance calculated from the equivalent circuit shown in Figure 4.3. Assuming $R_d > R_L > R_s$ the short circuit response time is roughly:

$$\tau = R_L C_d \sim 2 \times 10^{-10} \text{ s} \qquad (4.7)$$

with a typical 50-ohm load resistance. This response time should decrease when the diode is reversed biased. Providing the junction resistance remains larger than the load resistance, the photodiode frequency response should not change appreciably at a high operating temperature since the mobility and lifetime are not particularly sensitive to temperature over the 77 to 140°K temperature range.

To summarize the discussion of response time limitations, the photodiode should be capable of transit time limited operation exceeding the desired frequency response (400 MHz). The limiting transit time for carriers generated at the surface to diffuse to the junction is $\sim 1 \times 10^{-10}$ s. Due to the high absorption coefficient, only an insignificant number of carriers is generated in the n-type region where they take longer to reach the junction. With a 50-ohm load resistance terminating this diode, the relaxation time of charge stored by the depletion layer capacitance should be comparable to the transit time. Thus, with proper layout and package design, the photodiode as envisioned should exhibit the desired frequency response.

4.3.4 NOISE MECHANISM, NEP, D*

There are three sources of noise which contribute to the total noise current $\sqrt{\langle i_N^2 \rangle}$ at high modulation frequencies: shot (saturation) noise, thermal/Johnson noise, and background noise. These currents are independent of each other; and thus, the total noise current is the rms sum of these currents. There also should be a 1/f noise current in this diode; however, at high modulation frequencies this noise should be insignificant.

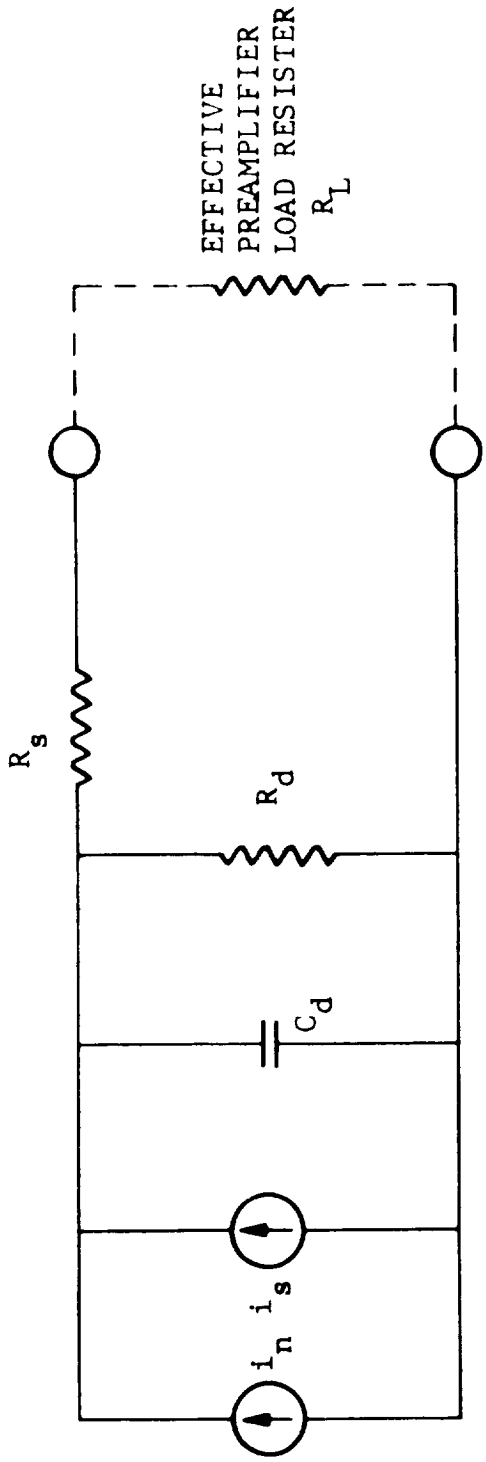

Figure 4.3 SMALL SIGNAL EQUIVALENT CIRCUIT
FOR PROPOSED PHOTODIODE

Shot noise is the result of the discreteness of electronic charge, and the current flowing through the device is the result of current pulses produced by the individual electronics and holes. The mean square value of this noise current is

$$\langle i_N^2 \rangle_{shot} = 2qAJ\Delta f \qquad (4.7)$$

The temperature dependence of this noise current increases roughly as $e^{-Eg/kT}$ with increasing temperature. At zero bias this noise current reduces to the thermal (Johnson) noise generated by the zero bias diode resistance. Assuming a diffusion limited saturation current and no surface conductance, this noise current at 77°K with the assumed device parameters is roughly 4×10^{-24} amp^2 in a 1-Hz bandwidth.

The detector responds also to the radiation emitted by the background and this results in an effective mean square noise current

$$\langle i_N^2 \rangle_{background} = 2\, q^2\, \eta\, J_r\, A\, \Delta f \qquad (4.8)$$

Assuming a 300°K background 180-degree field of view, 11-μm cutoff wavelength, and 0.2-quantum efficiency, this current is approximately 2×10^{-24} amp^2. Thus, at 77°K the shot and background noises are comparable.

The open circuit noise equivalent power calculated from the detector parameters and the sum of the above noise currents is

$$NEP_\lambda = \frac{hc}{q\,\lambda\,\eta} \sqrt{\langle i_N^2 \rangle / \Delta f} \approx 10^{-12} \text{ watts Hz}^{-1/2} \qquad (4.9)$$

The detectivity is

$$D^*_\lambda = \frac{\lambda\, q\, \eta \sqrt{A}}{hc \sqrt{\langle i_N^2 \rangle / \Delta f}} \approx 2 \times 10^{10} \text{ cm Hz}^{1/2}/\text{watt} \qquad (4.10)$$

Figure 4.4 shows the temperature dependent NEP and detectivity as a function of temperature calculated from the temperature dependence of the reverse bias current (Figure 4.2) and the assumed temperature independent sensitivity. However, it should be emphasized that high performance can be achieved when the photodiode is operated in the coherent detection mode. In heterodyne detection with a large local oscillator signal, the sensitivity of the device is considerably greater than in straight detection because of the high conversion gain between power at the input and at the difference frequency.

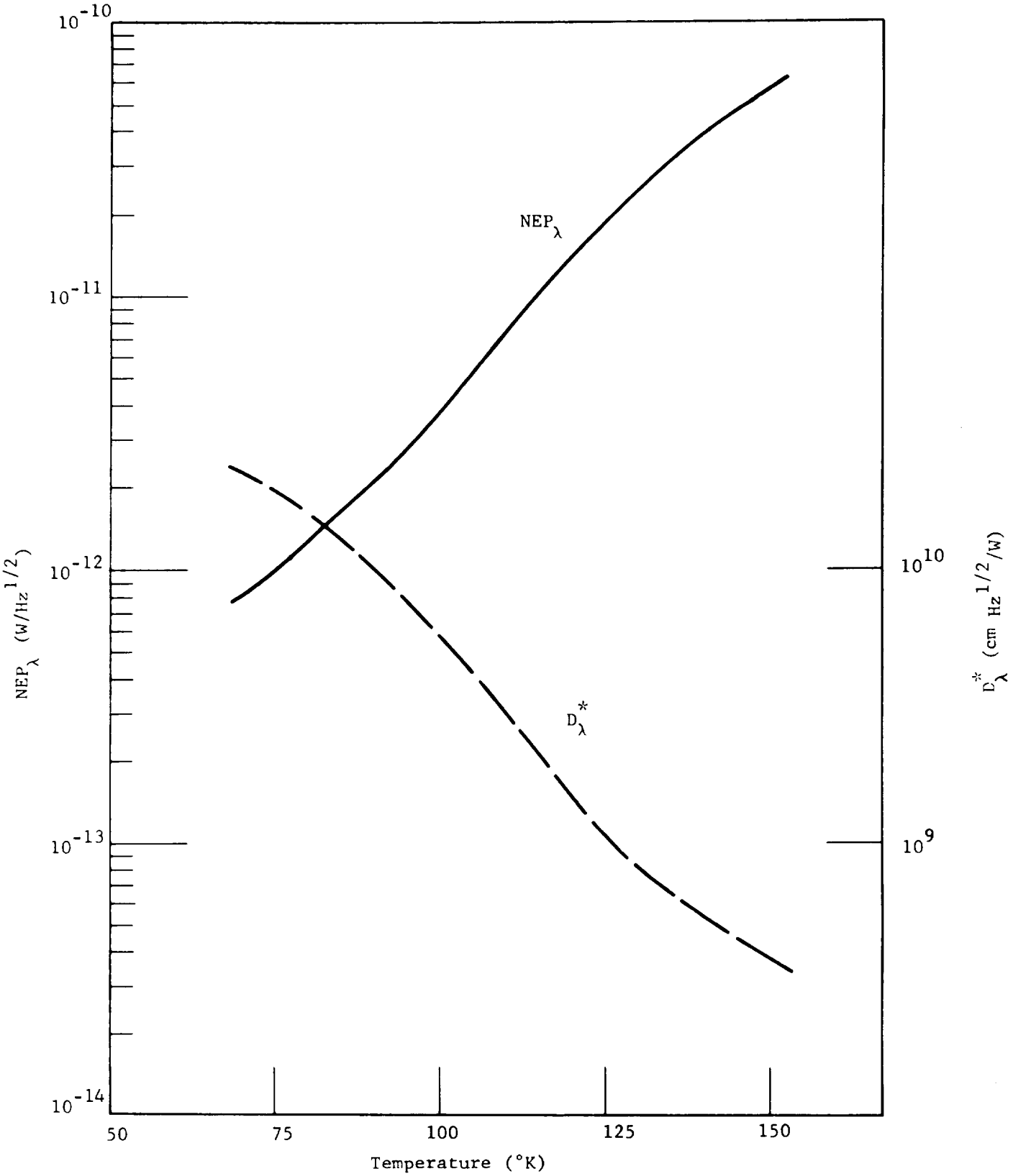

Figure 4.4 CALCULATED NEP_λ and D^*_λ VS TEMPERATURE AT (Hg,Cd)Te PHOTODIODE

SECTION 5

FABRICATION AND CHARACTERIZATION OF INITIAL DEVICES

Two approaches have been pursued in the advanced development of high speed (Hg,Cd)Te photodiodes for the detection of 10.6-μm radiation. The first, utilizing an acceptor impurity (gold) diffusion in n-type material, is an extension of the successful technology developed by Honeywell for near infrared photodiodes. The second utilizes the deviation from stoichiometry (mercury in and out diffusion) for p-n junction formation. Photodiodes have been fabricated by both techniques and their performance evaluated. Although neither technique has been fully exploited, it appears that as fabricated n-on p-type photodiodes with the low resistivity shallow diffused layers have a higher electrical bandwidth. The gold diffused photodiodes have high quantum efficiencies, however, the high series resistance of the experimental ring contact on the high resistivity p-type layer limits its frequency response through the RC product. The series resistance can be reduced with a different contact configuration such as the stripe pattern shown in Figure 4.1.

The initial criterion for a successful diode was the shape of the I-V characteristic at 77°K, as determined on an oscilloscope curve tracer. Diodes which exhibited rectifying characteristics were subjected to a series of subsequent measurements, including capacitance as a function of voltage; response to a pulsed fast-rise time GaAs laser and heterodyned CO_2 lasers; spectral response over the range 2-14 μm; and D_{BB}^* (500K, 1000, 1). From the D* measurements, responsivity and quantum efficiency were calculated.

Most of the gold and mercury diffused photodiodes exhibited a junction resistance lower than anticipated. Furthermore, in all cases, the reverse-bias current failed to saturate or follow the voltage dependence expected assuming space charge generation in the depletion layer. The reverse characteristics in many cases were relatively insensitive to temperature. Finally, the junction capacitances were very large and frequently exhibited anomalous voltage dependences. This phenomenon is possibly the result

of heavy doping concentrations in both sides of the junction or a non-planar diffusion. In view of these difficulties, much of the experimental effort was for diagnostic purposes.

5.1 GOLD DIFFUSED PHOTODIODES

5.1.1 Preparation

Gold has been diffused into n-type (Hg,Cd)Te material from ingots 40470, 10968 and 20968. A thin layer of gold is deposited over one surface of the (Hg,Cd)Te material using a dilute gold chloride solution. After diffusions ranging from 15 minutes to 8 hours at 275 to 300°C, the surface layer at 77°K thermoelectrically probes p-type consistently(see Section 4.2).

After the diffusion, the p-type surface, which becomes the active area, was lightly lapped to remove the excess gold and etched in bromine alcohol. For ohmic contact to the diffused region, gold and indium were deposited usually in a ring contact, however, a variety of other configurations were also employed for junction evaluation studies. The ring configuration was chosen to minimize the series spreading resistance in the shallow p-type layer. The area surrounding the contact ring is air abraded and etched to form a mesa structure as shown in Figure 5.1. These small arrays were mounted in evacuated dewars for temperature dependent evaluation measurements.

5.1.2 P-N Junction Characteristics

The initial investigation of gold diffusion in n-type (Hg,Cd)Te used material from ingot 20968 possessing the temperature dependent Hall coefficient and resistivity as shown in Figure 2.6. Although the surface region thermoelectrically probed p-type after diffusion consistent with the theory of gold diffusion (see Section 3.2), no rectifying current-voltage characteristics were obtained on a variety of diodes fabricated from such material. Since this gold diffusion technique has worked successfully in near infrared (1-5μm (Hg,Cd)Te), the gold diffusion was investigated in an intermediate composition of (Hg,Cd)Te material from ingot 40470. Figure 5.2 shows the current-voltage characteristics of such photodiodes measured at several temperatures with and

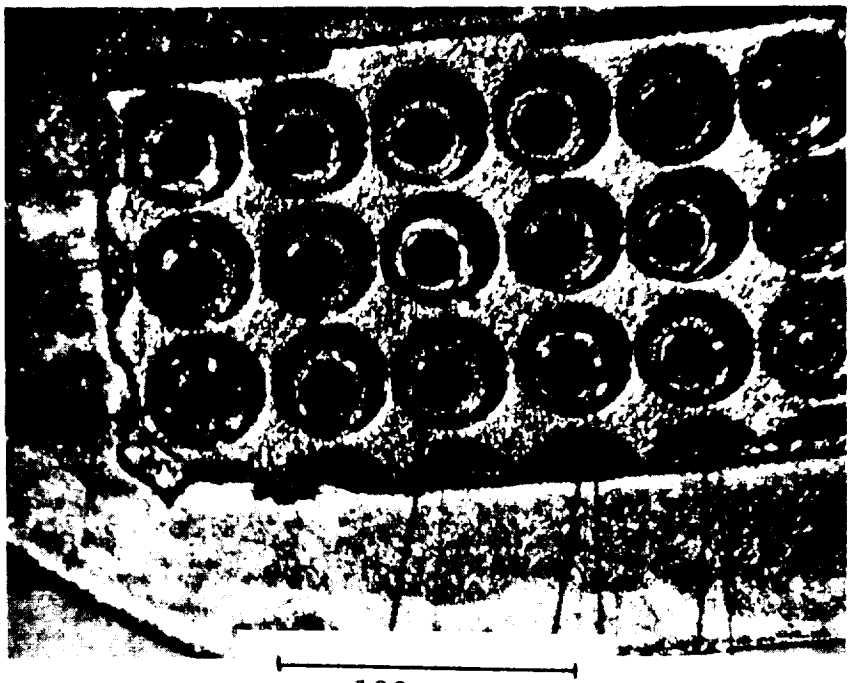

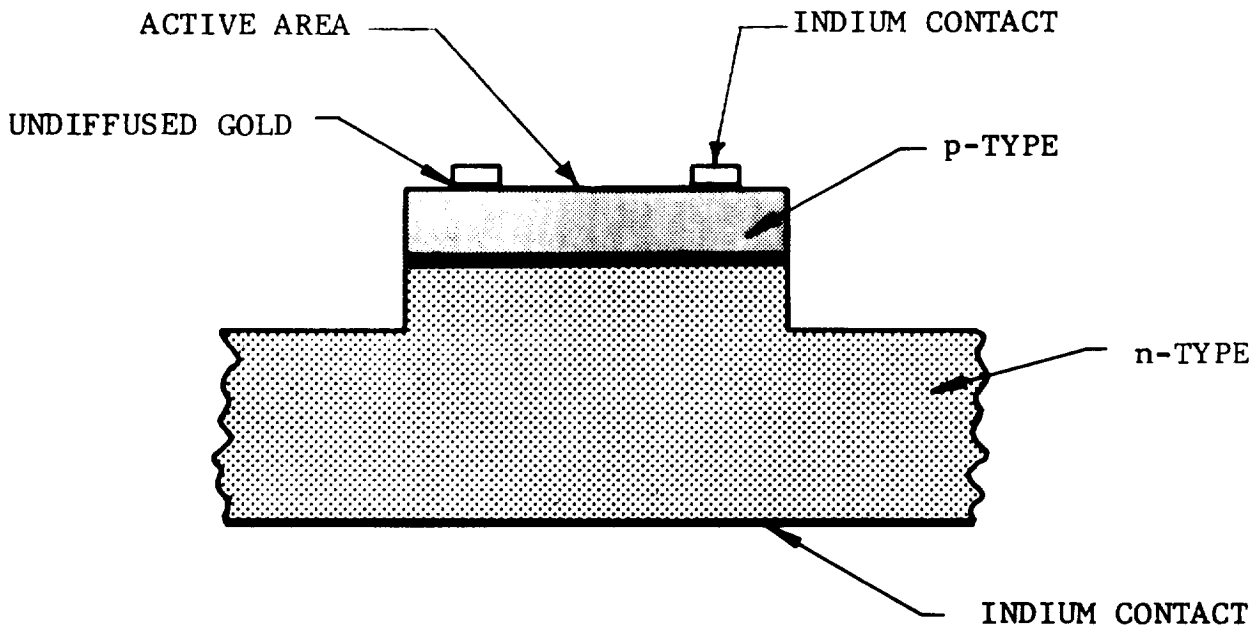

Figure 5.1 EXPERIMENTAL MESA PHOTODIODES FABRICATED IN (Hg,Cd)Te USING PHOTOLITHOGRAPHIC TECHNIQUES

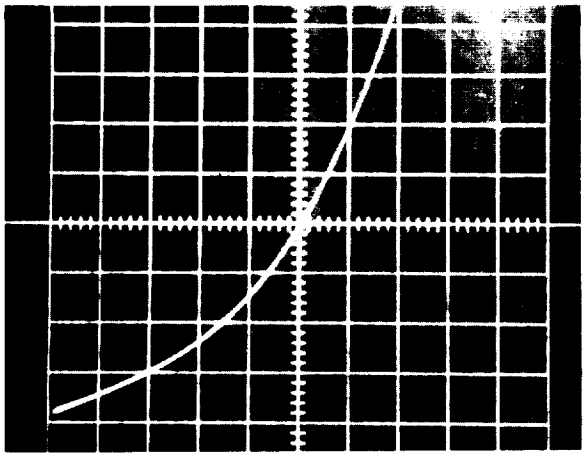

Area ~ 4 x 10^{-3} cm^2

(1) ~ 146°K
500 μA/cm
0.05 V/cm

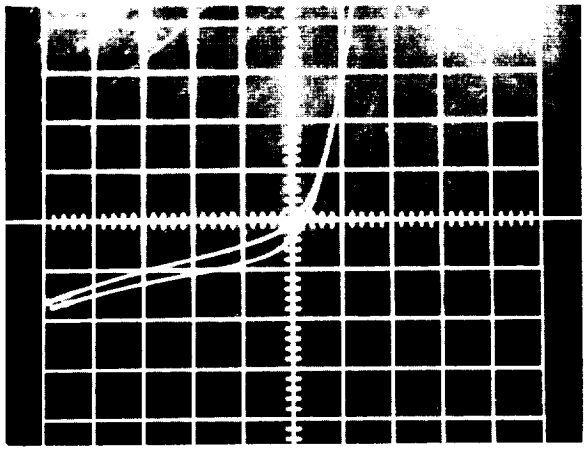

(2) ~ 90°K
100 μA/cm
0.05 V/cm

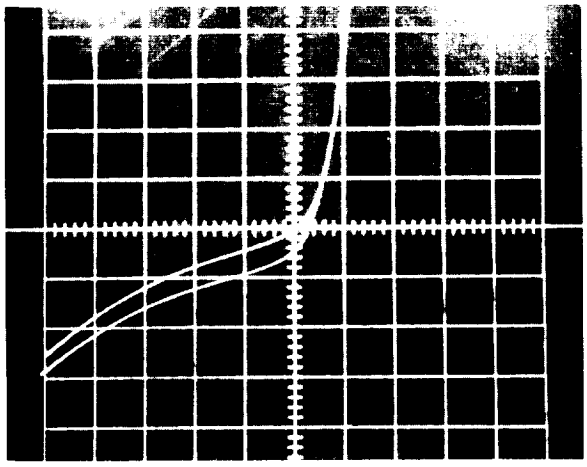

(3) ~ 77°K
50 μA/cm
0.05 V/cm

Figure 5.2 CURRENT VOLTAGE CHARACTERISTICS OF A GOLD DIFFUSED (Hg,Cd)Te PHOTODIODE AT SEVERAL TEMPERATURES WITH AND WITHOUT INCIDENT RADIATION (λp=7.4 μm) DIODE AREA 4 x $10^{-3}$$cm^2$ IDENTIFICATION NO. 40470 S161 F-3

without incident radiation. The energy gap of this material as determined by the peak spectral response is ϵg = 0.17 eV(λp=7.4μm). At 146°K the material is partially intrinsic and the current-voltage characteristics show only a small nonlinearity. At lower temperatures (90 and 77°K) the diode has a more pronounced rectifying characteristic, although the reverse bias current is larger than that calculated from estimated material parameters assuming dominant space charge generation currents. It is possible that the gold diffusion could have substantially degraded the lifetime, increasing the space charge generation current.

The capacitance was measured as a function of reverse bias to determine the doping profile. Figure 5.3 shows the voltage dependence of the shunt capacitance and resistance measured using a 1-MHz Boonton Capacitance Bridge (Model 78A) with a X1000 range extender required for the low shunt resistances. The reciprocal square of the capacitance varies linearly with low values of the applied voltage and extrapolates to a 45-mV contact potential. Figure 5.3 shows the variation of capacitance with the square root of the voltage corrected for the contact potential. Thus, the brief (5 minute) gold diffusion yielding a 10-μm estimated junction depth, has resulted in an abrupt p-n junction. However, there is a discrepancy in the acceptor doping concentration and contact potential calculated from the initial material parameters.

With the renewed confidence in the gold diffusion approach, several samples of n-type (Hg,Cd)Te from ingot 10968 having a peak resistivity in the 11 to 12-μm spectral range and a similar temperature dependent Hall coefficient and resistivity as shown in Figure 2.6 were given a brief gold diffusion. One sample, designated (H), was diffused in a flowing atmosphere of nitrogen and hydrogen. The other sample, designated (G), was sealed in a 0.3-cm^3 quartz tube. Since the junction depth is a function of the Hg partial pressure during diffusion, it is believed that these approaches should enhance the proportion of electrically active gold (presumed to be substitutional in Hg sites) yielding a shallow abrupt p-n junction. The junction depth was measured by thermoelectrically probing and lapping the diffused surface of an adjacent sample which was similarly diffused and is believed to be in the 10-to 30-mil range. Two evaporated indium contacts were made to the p-type surface layer on each mesa photodiode with

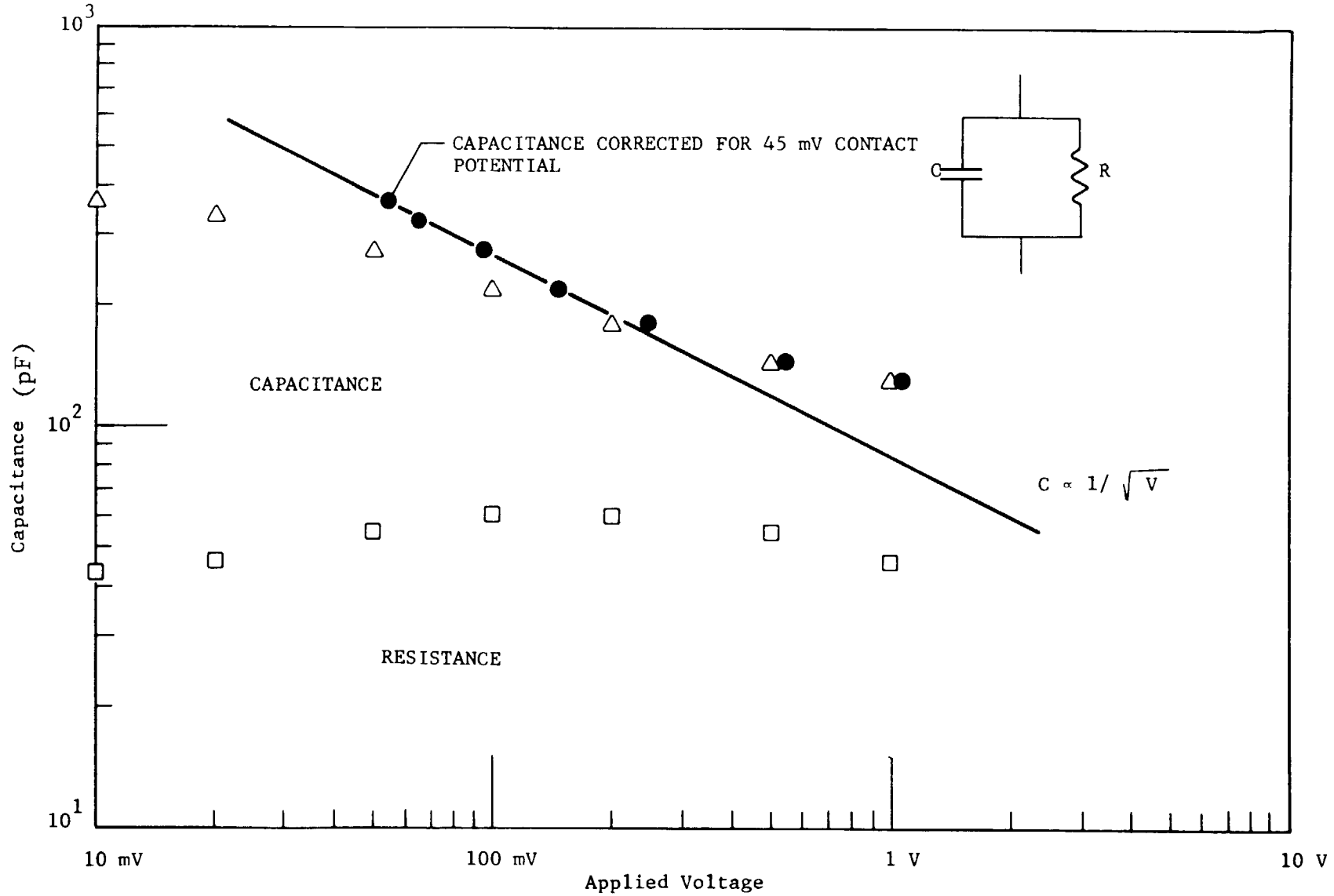

Figure 5.3 CAPACITANCE AND RESISTANCE OF A GOLD DIFFUSED (Hg,Cd)Te PHOTODIODE MEASURED AT 77°K DIODE AREA 3 x 10^{-3}cm^2 IDENTIFICATION No.40470 S161F-3

area 3 x 10^{-4} cm^2. The mesas were delineated by a brief air abrasion and chemical etching in a bromine methanol solution.

Figure 5.4 shows the measured current-voltage characteristics of a gold diffused photodiode at several temperatures. The reverse bias characteristics do not exhibit a saturation current, but rather are characterized by a shunt resistance of approximately 70 ohms at both 77 and 90°K. At higher temperatures, 146°K, the material becomes intrinsic and the junction characteristics become less pronounced. At lower temperatures, the forward bias injection effects are diminished and the current-voltage characteristics become almost linear with a 400 ohm resistance at 4.2°K.

Although the current-voltage characteristics between adjacent contacts on one mesa are similar to the reverse bias diode characteristics, the conductance and capacitance of the two contacts connected together relative to the base are approximately the same as either individual contact to the base. Thus, one can conclude that the entire surface of the mesa is high resistivity p-type and that the surface conductance is lower than the bulk n-type conductance including the junction resistance.

The capacitance of these diodes is insensitive to low values of applied reverse bias voltage due to the large contact potential, however, above 100mV it decreases almost linearly. Figure 5.5 shows the measured capacitance and resistance for one of the best gold diffused photodiodes at 77°K. There is no appreciable change for 90°K operation.

5.1.3 Sensitivity and Quantum Efficiency

Spectral response measurements as shown in Figure 5.6 were made on several photodiodes using a Beckman IR 604 spectrophotometer. Most of the 10968 S117 G and H photodiodes exhibited a peak response at 11.5μm at 77°K. At 90°K the peak responsivity is shifted to approximately 11.0μm.

Absolute responsivity and detectivity were measured using a 500°K blackbody chopped at 1kHz. The responsivity and small signal junction resistances as shown in Figure 5.6 are functions of the reverse bias voltage. The maximum blackbody responsivity of

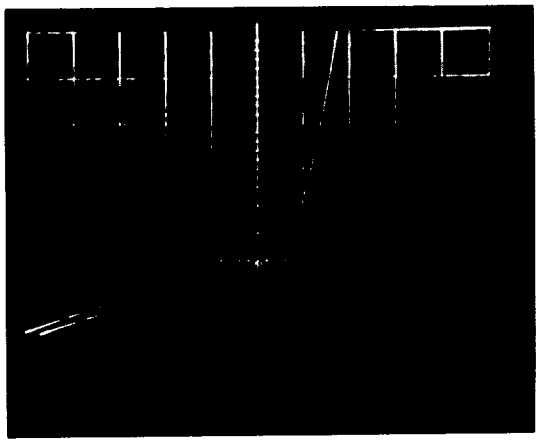

77°K

0.1/V/cm
5 mA/cm
with/without light

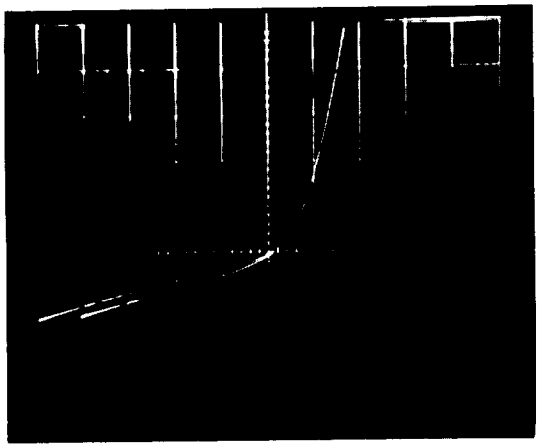

90°K

0.1 V/cm
5 mA/cm

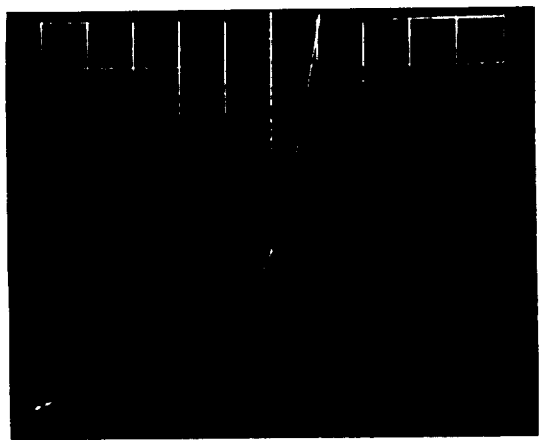

146°K

0.1 V/cm
5 mA/cm

Figure 5.4 CURRENT-VOLTAGE CHARACTERISTICS OF A GOLD DIFFUSED (Hg,Cd)Te PHOTODIODE AT SEVERAL TEMPERATURES WITH AND WITHOUT INCIDENT RADIATION, DIODE AREA $3 \times 10^{-3} cm^2$. IDENTIFICATION NO. 10968 S117 H

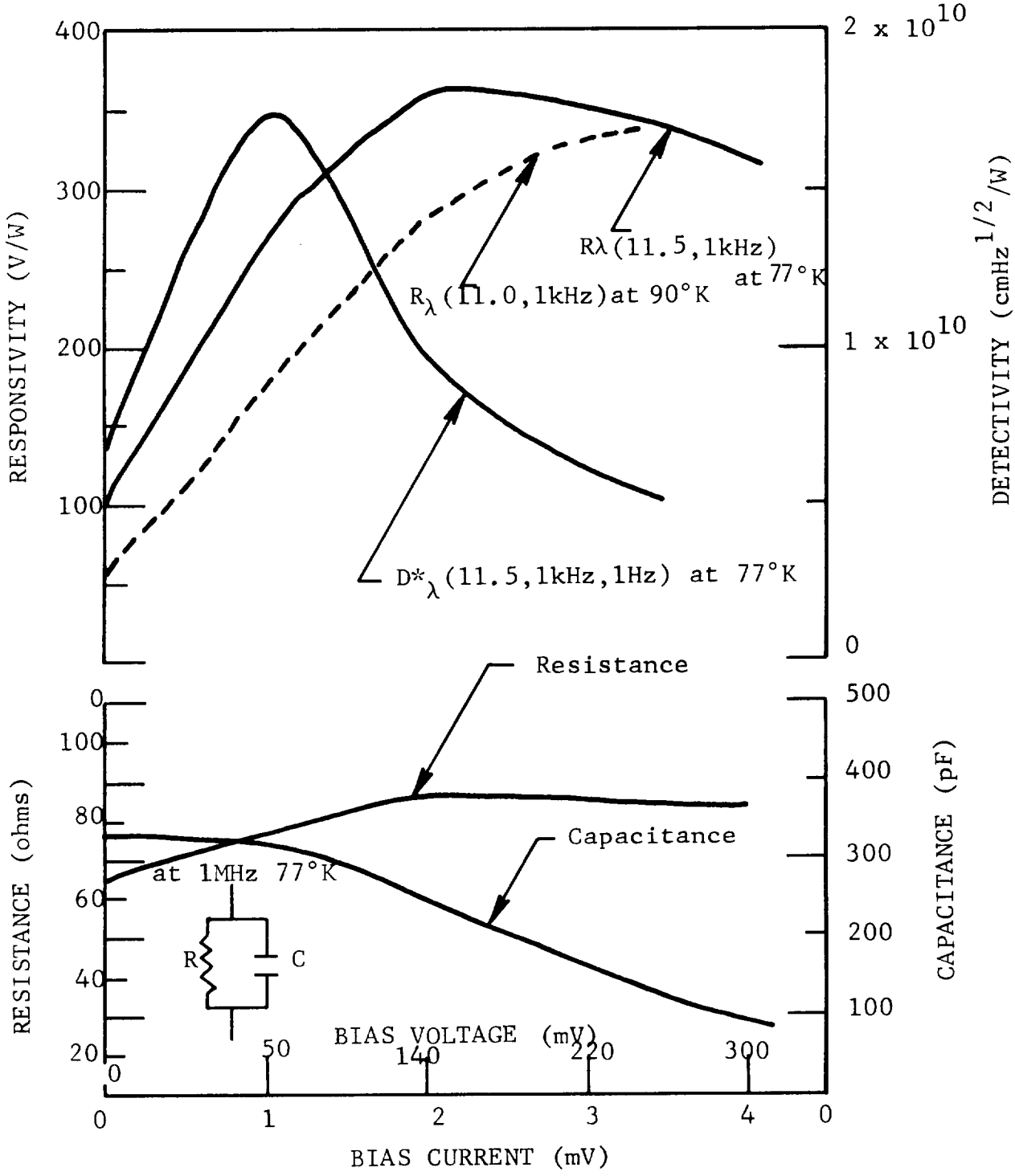

Figure 5.5 OPEN CIRCUIT RESPONSIVITY AND DETECTIVITY OF A FUNCTION OF REVERSE BIAS CURRENT FOR A GOLD DIFFUSED (Hg,Cd)Te PHOTODIODE (AREA = 3 x 10^{-3} cm^2, IDENTIFICATION NO. 10968-S117 H)

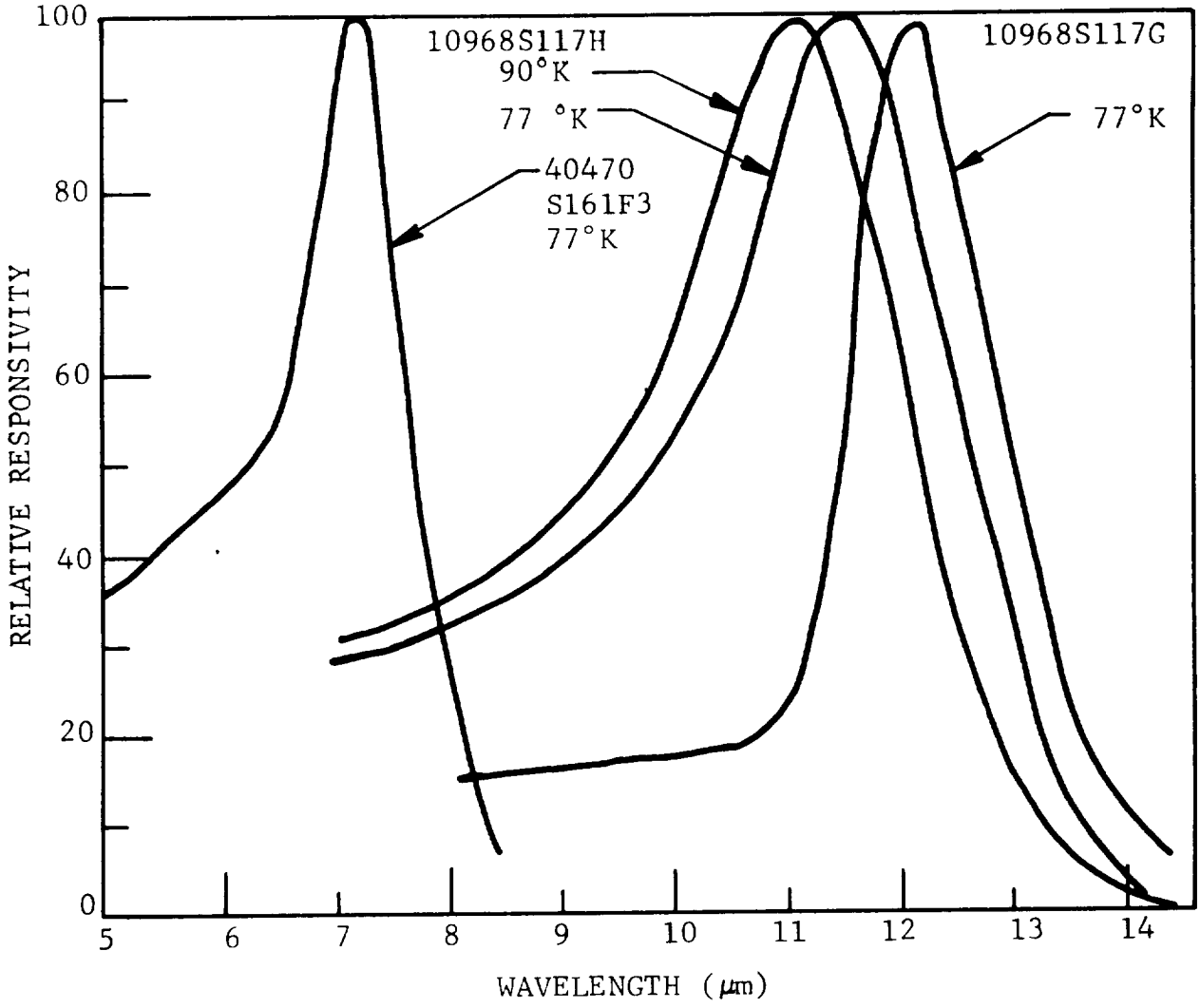

Figure 5.6 SPECTRAL RESPONSIVITY FOR SEVERAL GOLD DIFFUSED PHOTODIODES

10968 S-117 H photodiodes is approximately 160V/W at 77 and 90°K which occurs at roughly 0.2 volt reverse bias. The zero bias responsivity is nearly a factor of three smaller. The G factor for an ideal photon detector is 2.3 Thus, the peak spectral responsivity is at least 360V/W. Dividing the responsivity by the junction resistance yields a 5.2-A/W sensitivity (50% external quantum efficiency). The zero bias sensitivity measured with a 20-ohm load resistor is 1.7 A/W (16% external quantum efficiency). Since the responsivity increases with voltage faster than the junction resistance, it appears that the blackbody radiation forward biases the unbiased diode, decreasing the junction resistance and collection efficiency. The current-voltage characteristics as observed on a curve tracer do change substantially when the diode is in 77°K equilibrium or with incident room temperature background radiation. The spectral detectivity D_λ^* is $1.7 \times 10^{10} cmHz^{1/2}$ with the thermal noise generated in the shunt resistance, the dominant source of noise. Less extensive measurements were made on gold diffused photodiodes (10968-S117 G); however, their zero bias detectivity and responsivity are comparable to the H photodiodes.

Blackbody measurements were made only at zero reverse bias on 40470 S161F3 photodiodes. The open circuit blackbody responsivities are approximately 20 V/W. With a 3.3 σ factor, the peak spectral responsivity is approximately 70 V/W . The responsivity should increase with reverse bias voltage dividing the responsivity by the zero bias junction resistance yields on approximate 0.2 A/W sensitivity, corresponding to a 3% external quantum efficiency. The noise is obscured by the preamplifier system noise, but the $D^*_\lambda = 7.3\mu m > 5 \times 10^9 cmHz^{1/2}/W$. Assuming the photodiode is thermal noise limited, as occurs with other long wavelength (Hg,Cd)Te photodiodes, the detectivity at $\lambda p = 7.4\mu m$ should be $5 \times 10^{10} cmHz^{1/2}/W$.

5.1.4 Response Time

Response time measurements have been made on the gold diffused photodiodes using a pulsed GaAs laser diode emitting 0.9 μm radiation. Although 0.9 μm radiation is beyond the intended spectral range of the 7 and 11 μm photodiodes, the detected waveforms yield worst case information on the photodiode response

time. The detected waveform using 10968 S-117 H photodiodes at 77°K with 1mA reverse bias current has approximately a 40-nanosecond fall time constant* probably limited by electrical circuit constraints through the product of the junction capacitance and resistance. The zero bias fall time of 40470 S-161F-3 photodiodes at 77°K is longer, roughly 80 nanoseconds. Smaller area photodiodes with smaller capacitance and a 50-ohm input impedance preamplifier should substantially increase the bandwidth.

5.2 MERCURY DIFFUSED PHOTODIODES

5.2.1 Preparation

Mesa type diodes were fabricated from samples of initially p-type (Hg,Cd)Te material which were given various diffusion treatments as discussed in Section 3. Only samples having an n-type surface layer (determined by thermoelectric probing at 77°K and occasional Hall and resistivity measurements) were processed. The configuration and fabrication process follows those employed with the gold diffused photodiodes.

5.2.2 P-N Junction Characteristics

The current voltage (I-V) characteristics of all diodes were measured at 77°K, while more extensive temperature dependent measurements over the 9.5 to 146°K temperature range were made on certain representative diodes.

Figures 5.7 and 5.8 show the current-voltage characteristics of two mercury diffused (Hg,Cd)Te photodiodes at 77°K. Note the shift in reverse bias current with incident radiation as expected from p-n junction theory (Section 4). Although the reverse bias current does not saturate and is larger than that calculated from known material parameters, the current-voltage characteristics exhibit definite injection in forward bias. Reverse bias resistancesare in the 50 to 150-ohm range.

*Time constant defined as the 0 to 1/e time duration

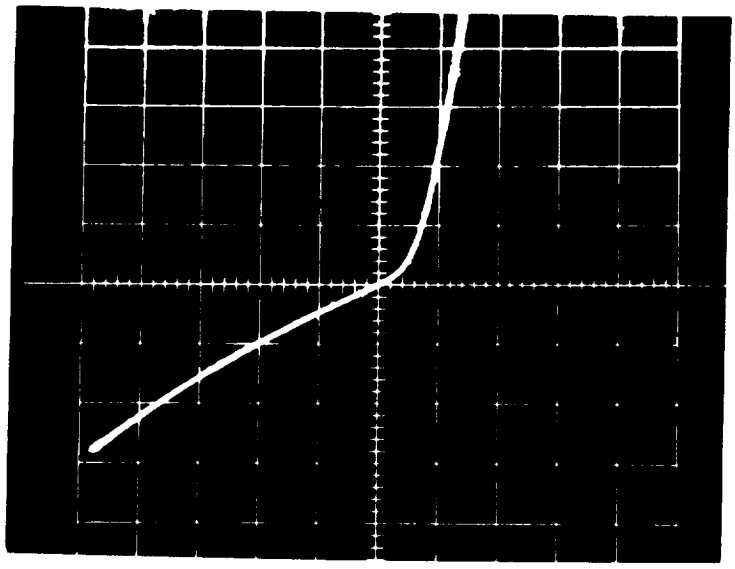

2 mA/cm

0.1V/cm

Figure 5.7 CURRENT-VOLTAGE CHARACTERISTICS OF A MERCURY DIFFUSED (Hg,Cd)Te PHOTODIODE AT 77°K (λp=8.5 μm) WITH AND WITHOUT INCIDENT RADIATION. DIODE AREA 3 x 10^{-3} cm^2. IDENTIFICATION No. 20769 S125 B-3

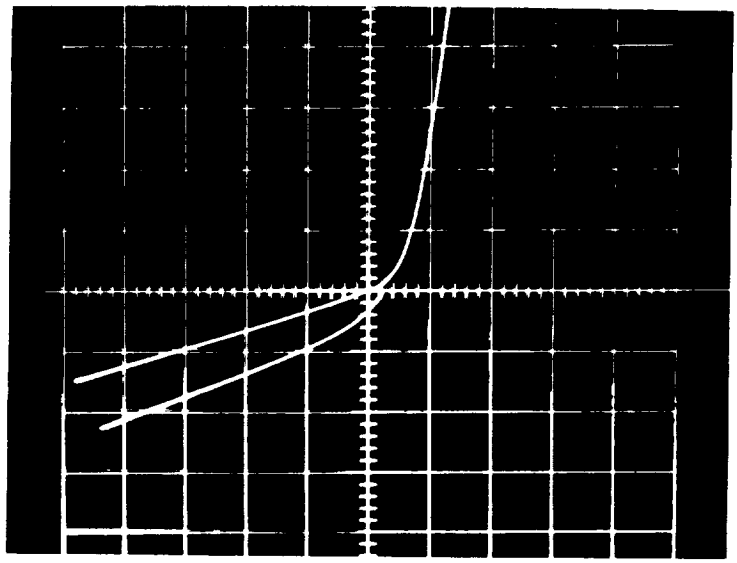

1 mA/cm

0.1 V/cm

Figure 5.8 CURRENT-VOLTAGE CHARACTERISTICS OF A MERCURY DIFFUSED (Hg,Cd)Te PHOTODIODE AT 77°K (λp=11 μm) DIODE AREA 3 x 10^{-3}. IDENTIFICATION NO.20769 S125 C-6

The temperature dependence of the current-voltage characteristics is shown in Figure 5.9. The left trace is at 77°K, while the origin is shifted 1 cm to the right for 90°K and 2 cm to the right for 156°K temperature operation. Note that the 77 and 90°K reverse bias currents and light sensitivities are similar.

Figure 5.10 shows the current-voltage characteristcs of a photodiode at several temperatures between 9.5 and 118°K. The reverse bias current decreases and forward bias injection becomes more pronounced as the temperature is reduced. However, at very low temperatures 34 and 9.5°K, there appears to be a definite change in diode characteristics which may be connected with the low temperature type conversion (positive to negative Hall coefficients) found in similar material.

The capacitance of thephotodiodes at 77°K has been measured as previously described in Section 5.1.2 Figure 5.11 shows the capacitance as a function of voltage for several representative photodiodes. Note the same sharp decrease in capacitance near 0.1-volt reverse bias. It is believed that the abrupt decrease is an extraneous effect due to a resonance in the range extender-dewar configuration which becomes dominant with low junction resistances.

The reverse characteristics of all mercury-diffused diodes deviate from that expected and are nearly linear with resistances ranging from 50 to 200 ohms. Several possible causes for this behavior have been postulated:

1) Surface leakage paths or channels

2) Non planar diffusion and diffusion "spikes"

3) Metallic precipitates which short circuit the junction space charge

4) Tunnel currents

5) Very short minority carrier lifetime coupled with a high density of recombination centers, such that currents are limited by ohmic scattering before diffusion or generation limiting is reached.

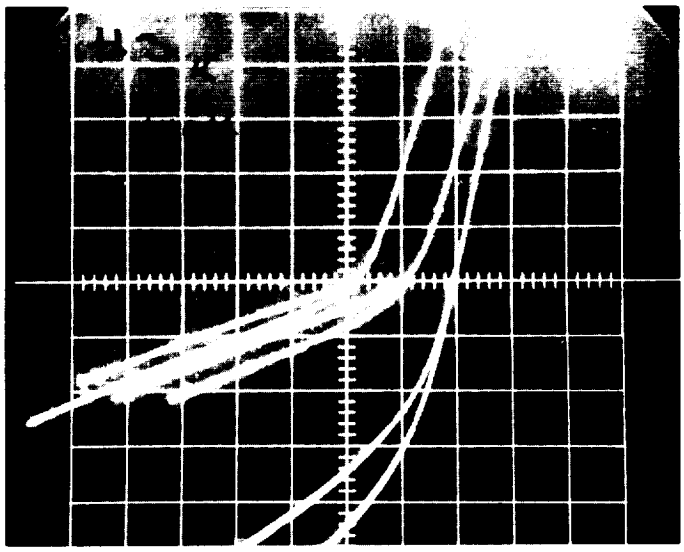

Figure 5.9 CURRENT-VOLTAGE CHARACTERISTICS OF A MERCURY DIFFUSED (Hg,Cd)Te PHOTODIODE AT SEVERAL TEMPERATURES WITH AND WITHOUT INCIDENT LIGHT

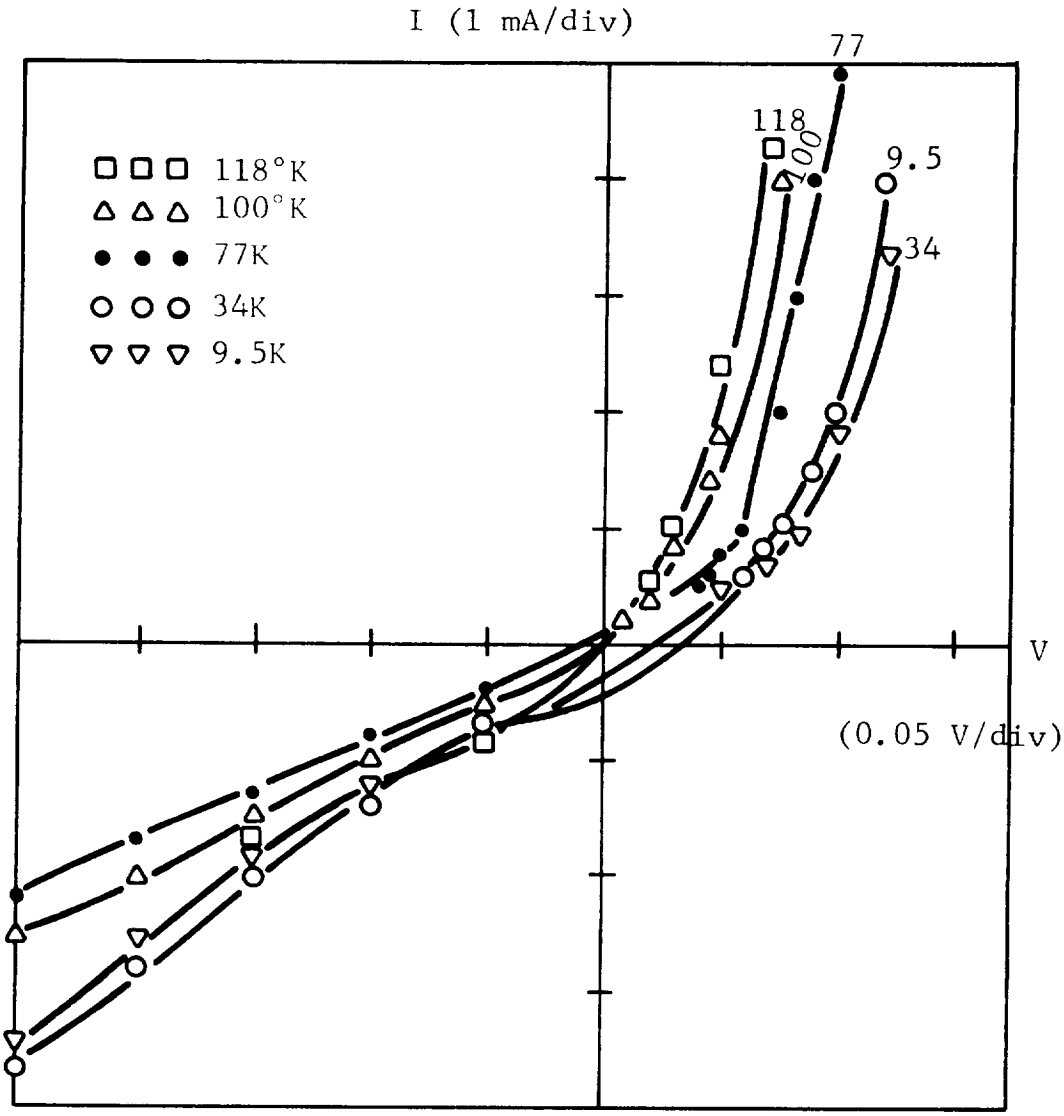

Figure 5.10 CURRENT-VOLTAGE CHARACTERISTICS OF A MERCURY DIFFUSED (Hg,Cd)Te PHOTODIODE AT SEVERAL TEMPERATURES ($\lambda p=8.5\mu m$) DIODE AREA 3×10^{-3} cm. IDENTIFICATION NO. 20769S125 B-3

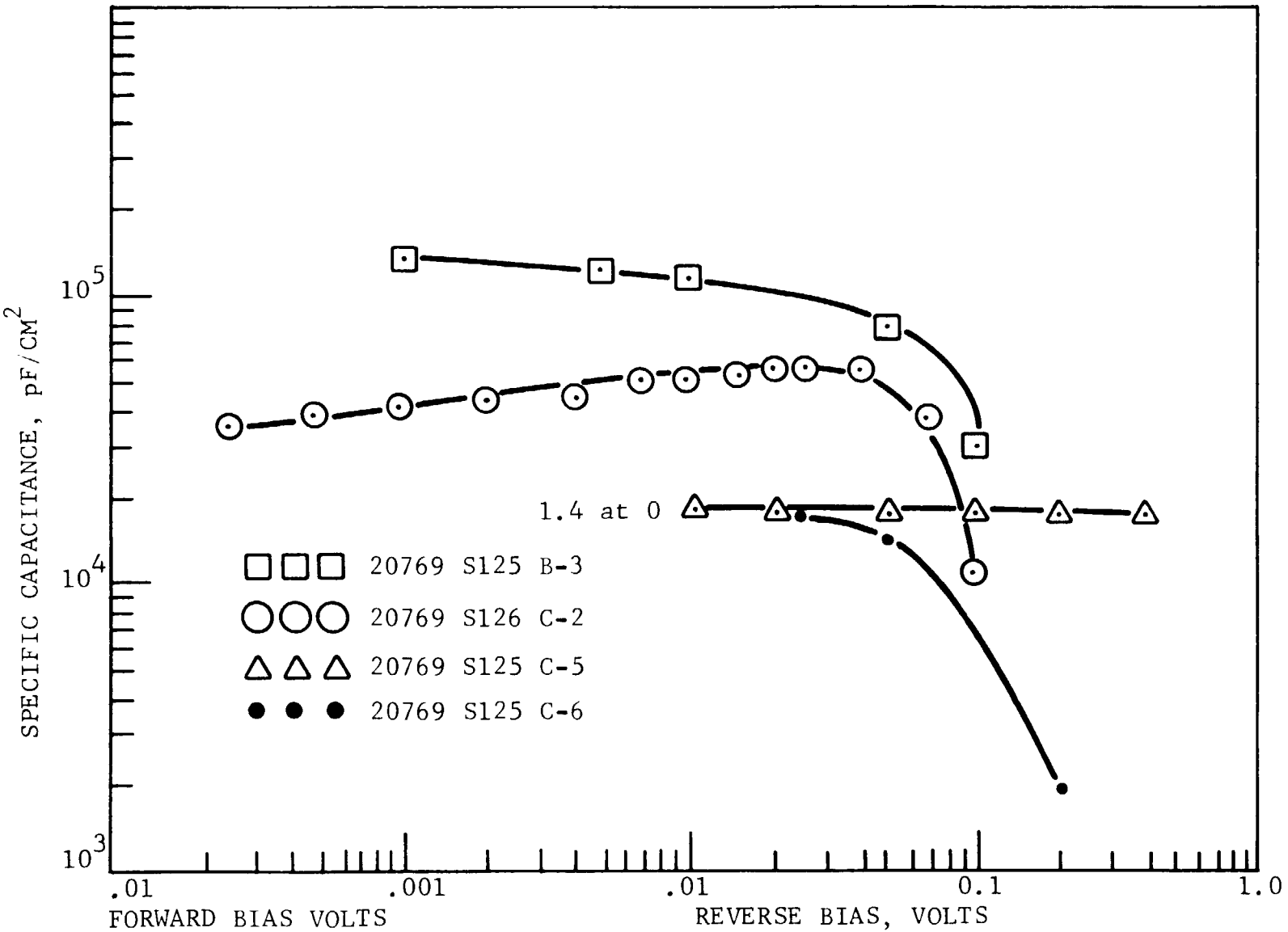

Figure 5.11 CAPACITANCE AS A FUNCTION OF VOLTAGE FOR SEVERAL MERCURY DIFFUSED (Hg,Cd)Te PHOTODIODES AT 77°K

However, it seems unlikely that the surface leakage paths or channels could result in such a low resistance which is insensitive to various surface treatments. Diffusion spikes and metal percipitates are quite possible based on the visual examination of the material which frequently has small mercury pits. Tunneling is believed to have been observed in at least one set of diodes 20769 S126C-1. It is possible that tunneling currents could contribute to the nearly temperature independent reverse bias current. The last possibility is based on a worst case calculation of the expected diffusion and space charge generation currents in the tens of milliamperes.

5.2.3 Sensitivity and Quantum Efficiency

Figure 5.12 shows the spectral response of two mercury diffused photodiodes at 77°K. The difference between these detectors is that C-5 is inverted with radiation incident on the p-type material, while C-6 has radiation incident on the n-type diffused layer. The broad spectral response with a gradual cut-off is expected in the deep junction C-5 photodiode.

The responsivity of the 20769 S125 BB photodiodes at zero bias is approximately 200 V/W. The quantum efficiency calculated by dividing responsivity by the diode resistance is approximately 4%. However, it is believed that substantially higher responsivities are possible when the photodiode is reversed biased and the active surface is etched after diffusion in the detector fabrication process. The characteristics of several mercury and gold diffused photodiodes are outlined in Table 5.1.

5.2.4 Response Time

The frequency response of these mercury diffused photodiodes has been investigated using a CO_2 laser (10.6 μm) heterodyne and pulsed GaAs laser diode (0.9 μm). Figure 5.13a shows the pulse waveform emitted by the GaAs laser diode as detected with an ultra high speed silicon PIN photodiode. Figure 5.13b shows the pulse response of a typical diode from B-3 (λ_p = 8.5 μm) at several bias levels. These diodes had a larger than anticipated junction capacitance in the 100 to 400 pF range due to the high doping concentration, and exhibited and RC limited frequency

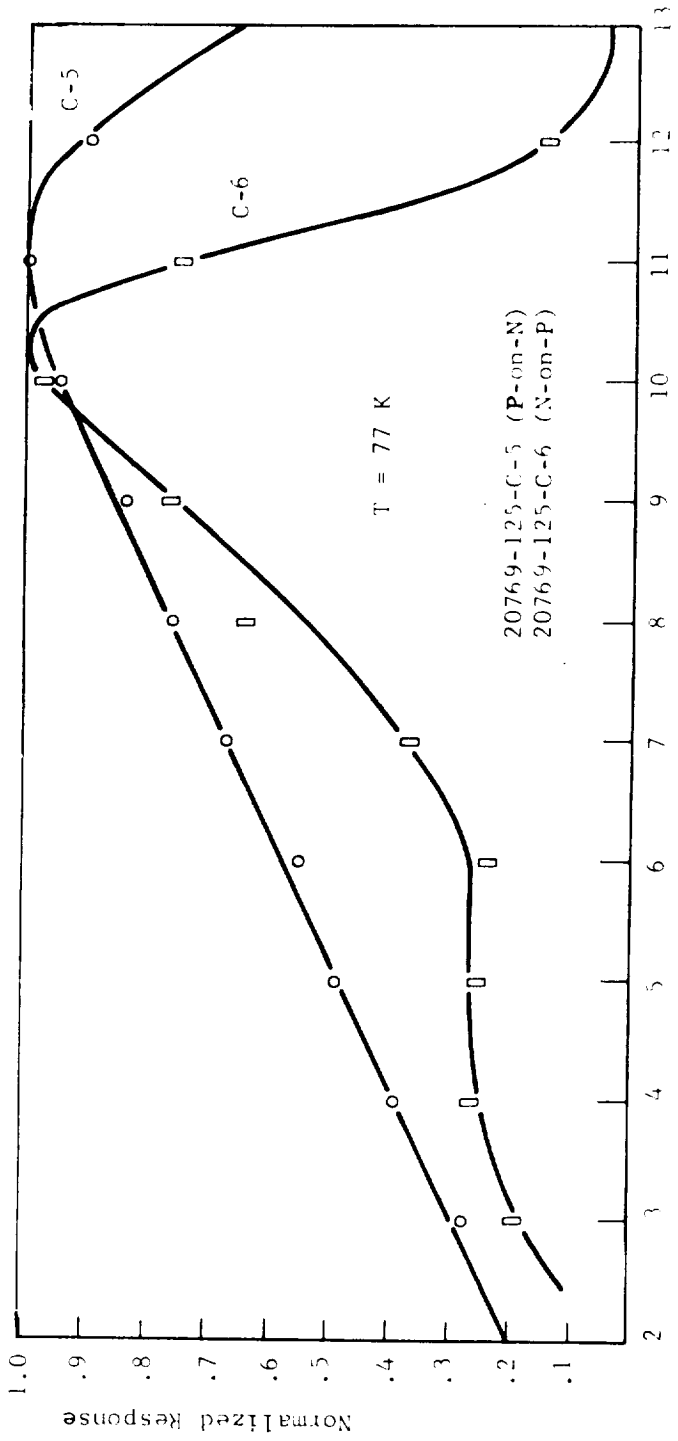

Figure 5.12 SPECTRAL RESPONSE OF TWO MERCURY DIFFUSED (Hg,Cd)Te FOR INFRARED PHOTODIODES

Table 5.1

CHARACTERISTICS OF (Hg,Cd)Te PHOTODIODES

DIODE NO.	JUNCTION DEPTH μm	λ_p μm	TOTAL AREA, CM^2	R_D, Ω, At 0.1V Bias 77K	90K	146K	CAPACITANCE pF/CM^2	$R\lambda$ V/W	η,%	D^*_λ cmHz 1/2 W^{-1}	τ ns
MERCURY DIFFUSED											
S125B31	15-35	8.6	3.4×10^{-3}	120			1.2×10^5	61*	7.3*	6×19^9*	20 ns at 0.9μm
	"	"	"	120				200*	24*	1.5×10^{10}*	
S125B33	"	"	"	120				206*	24*	1.5×10^{10}*	
S125C51		11.5	3.4×10^{-3}	45			3.5×10^4	65*	19*	$>7 \times 10^9$*	50 ns at 0.9μm 16 ns at 10.6μm
S125C61	130	10.3	3.4×10^{-3}	200			1.2×10^4	38*	2.3*	$>2 \times 10^9$*	
S126C2-1	10-35	10.1	3.4×10^{-3}	7.5				4.6 *	7.5	4.3×10^8*	
S126C2-3	"	"	"	43-60			1.2×10^4	37 *	7.6	3.6×10^9*	<7 ns at 10.6μm
S126C2-4	"	"	"	25				23 *	11	2.0×10^9*	
GOLD DIFFUSED											
40470S161F1	10-20	7.3	5×10^{-3}	400	-	300	4×10^4	63*	3*	$>4 \times 10^9$*	200 ns at 0.9μm
2	"			200			6×10^4	71*	6*	$>5 \times 10^9$*	
3	"			200			4×10^4	41*	3*	$>4 \times 19^9$*	
4	"		3×10^3	2.5K	2.0K	140	10×10^4	56*	1*		80 ns at 0.9μm
10968S117 G1	10-20	11.5	4×10^{-3}	50			6×10^4	-			
G2	"	11.5	4×10^{-3}	100			6×10^4	-			
10968S117 H1	10-20	11.5	4×10^{-3}	70	75	35	10×10^4	100*-360	16*-50	1.7×10^{10}	40 ns at 0.9μm
H2	"	11.5	4×10^{-3}	50			10×10^4	200			

* Zero bias (note definite increase in performance as shown in Figure 4.2.1 when reversed biased)

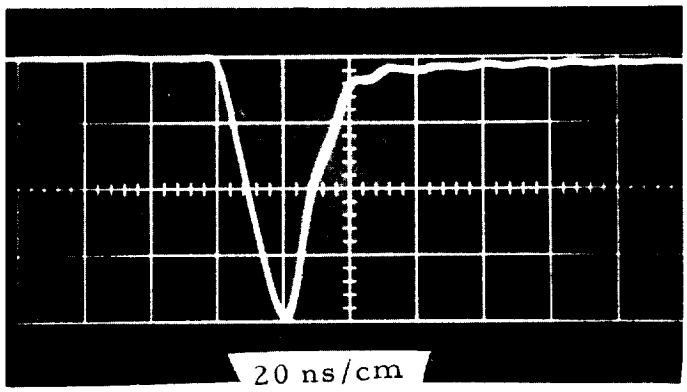

A IR PULSE SHAPE EMITTED FROM A GaAs LASER DIODE (0.9μm) AS DETECTED WITH A ULTRAFAST SILICON PIN PHOTODIODE

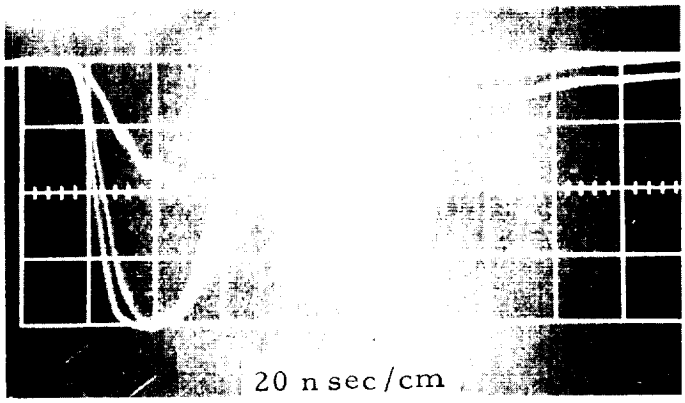

B PULSE RESPONSE OF 8.5μm(Hg,Cd)Te PHOTODIODE AT 77°K WITH VARIOUS BIAS CURRENTS 0, 0.5, 1.0, 1.5 mA TO 0.9μm RADIATION FROM GaAs LASER DIODE

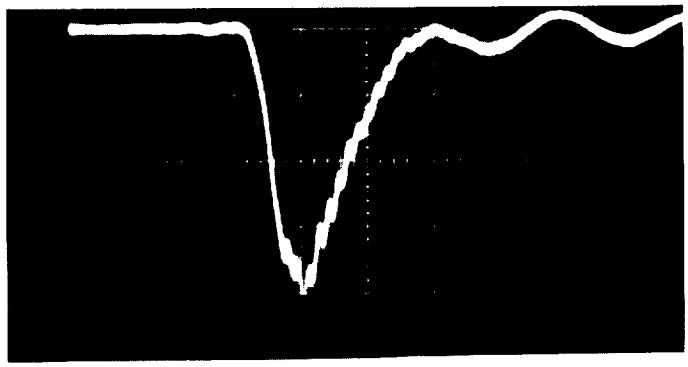

C PULSE RESPONSE OF 11μm (Hg,Cd)Te PHOTODIODE AT 77°K TO 0.9μm RADIATION

Figure 5.13

response in the 15 to 60 nanosecond range as shown. The capacitance of an 11-μm(Hg,Cd)Te C-6 photodiode is roughly 30 pF, and it exhibited a pulse response to 0.9 μm radiation shown in Figure 4.28c that was transit time limited less than 10 nanoseconds.

Initial CO_2 laser heterodyne frequency response measurements (λ = 10.6 μm) have been made on two photodiodes. Diode C-5 showed good response to approximately 10 MHz, at which frequency a decrease was observed. This roll-off frequency is in the range expected from the diode RC time constant, 16 MHz. Diode C-2 showed an almost constant response out to 25 MHz, which is the highest frequency obtainable with this system.

REFERENCES

1. J. L. Schmit and E. L. Stelzer, J. Appl. Phys., 40, 4865 (1969).

2. M. W. Scott, J. Appl. Phys., 40, 4077 (1969).

3. W. Saur, Honeywell Corporate Research Center, Internal Memo (October 1967).

4. F. Stern, "Elementary Theory of the Optical Properties of Solids," Solid State Physics, Vol. 15, pp 300-409, edited by F. Seitz and D. Turnbull. Academic Press, New York, 1963.

5. J. L. Schmit, J. Appl. Phys., 41, 2876 (1970).

6. E. O. Kane, J. Phys. Chem, Solids, 1, 249 (1957).

8. D. Soderman and M. Barnoski, Unpublished data measured at the Honeywell Radiation Center on $(Hg_{0.7},Cd_{0.3})Te$ at 77°K and Kinch and Buss, Proc. Conf. on Physics of Semimetals and Narrow-Gap Semiconductors, Dallas March 1970.

9. R. Lancaster, K. Button, B. Lax, T. Cronbury and D. Soderman "Quantum Effects in Cyclotron Resonance in n-type (Hg,Cd)Te," presented by K. Button at APS Meeting Dallas March 1970.

10. J. D. Wiley and R. N. Dexter, Phys. Rev., 181, 1181 (1969).

11. B. L. Musicant, Final Report for Infrared Photodetector Contract NAS5-11554, Honeywell Radiation Center June (1969).

12. M. W. Scott, Honeywell Corporate Research Center, Internal Memo April 1970.

13. C. Verie and J. Ayos, Appl. Phys. Letters, 10, 241 (1967).

14. R. C. Whelan and D. Shaw, II-VI Semiconducting Compounds 1967 International Conference (edited by D. G. Thomas), Benjamin, New York (1967).

15. E. Nebauer, Phys. Stat. Sol. 29, 269 (1968).

16. S. C. Choo, Solid State Electronics 11, 1069 (1968).

17. A. G. Jordan and A. G. Milnes, IRE Trans. ED___ 242 (1960).

18. V. J. Corcoran, R.E. Cupp, J.J. Gallagher, and W. T. Smith, Appl. Phys. Letter, 16, 316 (1970).